DTIC FILE COPY

AFOSR-TR- 89-0685

MINISTRY OF INDUSTRY & TRADE
INDUSTRIAL R & D ADMINISTRATION
משרד התעשיה והמסחר
המינהל למחקר ופיתוח תעשייתי

ISRAEL INSTITUTE OF METALS · מכון המתכות הישראלי

TECHNION RESEARCH AND DEVELOPMENT FOUNDATION LTD.
מוסד הטכניון למחקר ופיתוח בע"מ

AD-A208 873

(2)

Coating and Impregnation of Carbon-Carbon Composites with Ceramics by Electrophoretic Deposition

DTIC
ELECTE
JUN 07 1989
S D
D CS

L. Gal-Or, S. Liubovich
Israel Institute of Metals

FINAL
~~Interim~~ Scientific Report

March 1, 1988 — February 28, 1989

DISTRIBUTION STATEMENT A
Approved for public release
Distribution Unlimited

Prepared for
EOARD — England, London
AFOSR — Boiling, Washington, D.C., 20332, U.S.A.

89 6 06 030

UNCLASSIFIED
SECURITY CLASSIFICATION OF THIS PAGE

REPORT DOCUMENTATION PAGE

1a. REPORT SECURITY CLASSIFICATION Unclassified	1b. RESTRICTIVE MARKINGS
2a. SECURITY CLASSIFICATION AUTHORITY	3. DISTRIBUTION/AVAILABILITY OF REPORT Approved for public release; Distribution unlimited
2b. DECLASSIFICATION/DOWNGRADING SCHEDULE	
4. PERFORMING ORGANIZATION REPORT NUMBER(S)	5. MONITORING ORGANIZATION REPORT NUMBER(S) AFOSR-TR- 89-0685
6a. NAME OF PERFORMING ORGANIZATION Israel Institute of Metals 6b. OFFICE SYMBOL (If applicable)	7a. NAME OF MONITORING ORGANIZATION ~~European Office of Aerospace Research and Development~~ AFOSR/NE
6c. ADDRESS (City, State, and ZIP Code) Technion Research and Development Foundation Technion City Haifa 32000, Israel	7b. ADDRESS (City, State, and ZIP Code) ~~Box 14~~ BUILDING 410 ~~FPO New York 09510-0200~~ BOLLING AFB, DC 20332-6448
8a. NAME OF FUNDING/SPONSORING ORGANIZATION Air Force Office of Scientific Research 8b. OFFICE SYMBOL (If applicable) NE	9. PROCUREMENT INSTRUMENT IDENTIFICATION NUMBER AFOSR 88-0097
8c. ADDRESS (City, State, and ZIP Code) Bolling AFB, DC 20332-6448 SAME AS 7b	10. SOURCE OF FUNDING NUMBERS PROGRAM ELEMENT NO. 61102F; PROJECT NO. 2306; TASK NO. A2; WORK UNIT ACCESSION NO.

11. TITLE (Include Security Classification)
Coating and Impregnation of Carbon-Carbon Composits with Ceramics by Electrophoretic Deposition.

12. PERSONAL AUTHOR(S) L. Gal-Or, S. Liubovich

13a. TYPE OF REPORT	13b. TIME COVERED	14. DATE OF REPORT (Year, Month, Day)	15. PAGE COUNT
FINAL ~~Interim~~	FROM 3/1/88 TO 2/28/89	April 1989	85

16. SUPPLEMENTARY NOTATION

17. COSATI CODES			18. SUBJECT TERMS (Continue on reverse if necessary and identify by block number)
FIELD	GROUP	SUB-GROUP	Electrophoretic Deposition, Electrodeposition, Carbon-Carbon Composites, Coating, Impregnation.

19. ABSTRACT (Continue on reverse if necessary and identify by block number)

Electrophoretic deposition of ceramic coatings on porous graphite and on a 2D C-C composite was studied using colloidal and fused SiO_2, SiC and SiN. It was shown that all these ceramic materials acquire an electric charge and hence deposit under the influence of the electric field. In addition to the formation of a surface deposit, the induction of particles into the pores of porous graphite was demonstrated. The effects of deposition voltage, solvent properties and particle concentration on penetration were studied by examination of cross-sections in the SEM and by quantitative analysis of induced SiO_2. Ceramic deposits of CeO_2, ZrO_2 and Al_2O_3 were formed on graphite and 2D C-C by an electrochemical reduction of aqueous solutions containing inorganic salts of the appropriate metals. (JCS)

20. DISTRIBUTION/AVAILABILITY OF ABSTRACT	21. ABSTRACT SECURITY CLASSIFICATION
☒ UNCLASSIFIED/UNLIMITED ☐ SAME AS RPT. ☐ DTIC USERS	Unclassified
22a. NAME OF RESPONSIBLE INDIVIDUAL Dr. ~~Allen R. Rosenstein~~ CHARLOTTE J. SCHOLLER	22b. TELEPHONE (Include Area Code) (202) 767-4984 93
	22c. OFFICE SYMBOL AFOSR/NE

DD FORM 1473, 84 MAR 83 APR edition may be used until exhausted. All other editions are obsolete.

SECURITY CLASSIFICATION OF THIS PAGE
UNCLASSIFIED

COATING AND IMPREGNATION OF CARBON-CARBON COMPOSITES WITH CERAMICS BY ELECTROPHORETIC DEPOSITION

QUALITY INSPECTED 2

L. Gal-Or, S. Liubovich

Israel Institute of Metals

Accesion For
NTIS CRA&I ☑
DTIC TAB ☐
Unannounced ☐
Justification
By
Distribution/
Availability Codes
Dist | Avail and/or Special
A-1

AFOSR Grant 88-0097

Technion No. 5045-06

FINAL
~~Interim~~ Scientific Report

March 1, 1988 - February 28, 1989

Prepared for

EOARD - England, London
AFOSR - Bolling, Washington D.C., 20332, U.S.A.

Copyright C 1989 by L. Gal-Or, S. Liubovich, Israel Institute of Metals, Technion Res. & Dev. Foundation Ltd.

TABLE OF CONTENTS

CHPATER 1 - INTRODUCTION

The present report summarizes the work performed in the first stage of the project.

The final objective of this project is to develop a method for coating and impregnation of carbon-carbon composites with ceramic materials so as to enable their application in oxidising atmospheres at elevated temperatures.

The basic concept of the program is to utilize the phenomenon of electrophoresis, which has been so far applied extensively in biological systems, for the displacement of ceramic particles and their deposition on the C-C substrate. The electric conductivity of the C-C enables its functioning as an electrode in an electric circuit in which a high strength field is applied generating the motion of the charged ceramic particles. Moreover, it is expected that the high strength field will facilitate the penetration of the fine ceramic particles into residual pores and cracks of the substrate.

The scope of the project was later expanded so as to include a new method of deposition, in addition to electrophoresis - electroreduction. By this method ceramic oxides are synthesized from an ionic aqueous solution following an electrochemical reaction.

In the present stage most experiments were performed on a model material for C-C – porous graphite. The main reasons for the use of this model material are its more accurate characterization and hence better reproducibility, in addition to more ready avaiability.

As part of the general scope described above the following objectives were put forward for this stage:

- To investigate the possibility to charge, and hence deposit under the influence of the electric field, a number of ceramic materials which can potentially protect C-C in high-temperature oxidizing environments (colloidal and fused SiO_2, SiN and SiC).

- To investigate the possibility to deposit ceramic coatings on graphite and C-C from aqueous ionic solutions by electroreduction (the coatings studied were CeO_2, ZrO_2 and Al_2O_3).

- To prove the concept that ceramic particles can be induced into a porous substrate due to the effect of the electric field.

- To verify the possibility to obtain ceramic deposits in the pores of a porous substrate by electroreduction of a suitable ionic solution.

CHAPTER 2 - LITERATURE SURVEY

2.1 ELECTROPHORETIC DEPOSITION OF CERAMIC PARTICLES

Electrophoretic deposition of ceramic coatings has two main advantages when compared to other coating methods:

- more rigid control of coating thickness;
- better "throwing power" which enables efficient coating of complex shapes.

As related to our specific interest a third advantage seems attainable: the induction of the ceramic coating into the pores of a porous substrate under the influence of the electric field.

Electrophoretic deposition is obtained by the movement of non-conductive but electrically charged particles in an electric field to one of the electrodes.
Two different charging modes are attributed to ceramic particles [1]:

a) dissociation mode, such as the dissociation of silanol groups present in silica:
   $SiOH + OH^- \longrightarrow \equiv SiO^- + H_2O$ (negatively charged particles)
b) adsorption mode, such as the adsorption of H^+ from water or from weak acids: $n\ Al(OH)_3 + HNO_3 \longrightarrow [Al(OH)_3]_n \cdot xH^+ + xNO^-_3$ (positively charged particles).

The surface charge once formed is then balanced by ions of an opposite charge derived from the solution and thus a double layer is formed.

Usually the polarity of the particles has to be determined experimentally because the particles acquire the charge spontaneously when mixed with the solvent. Further, this charge may be reversed upon addition of ionic compounds.

According to the model proposed by Stern the double layer constitutes of a rigid part with a linear potential gradient,

and a diffuse part with a non-linear potential gradient termed "Zeta potential".

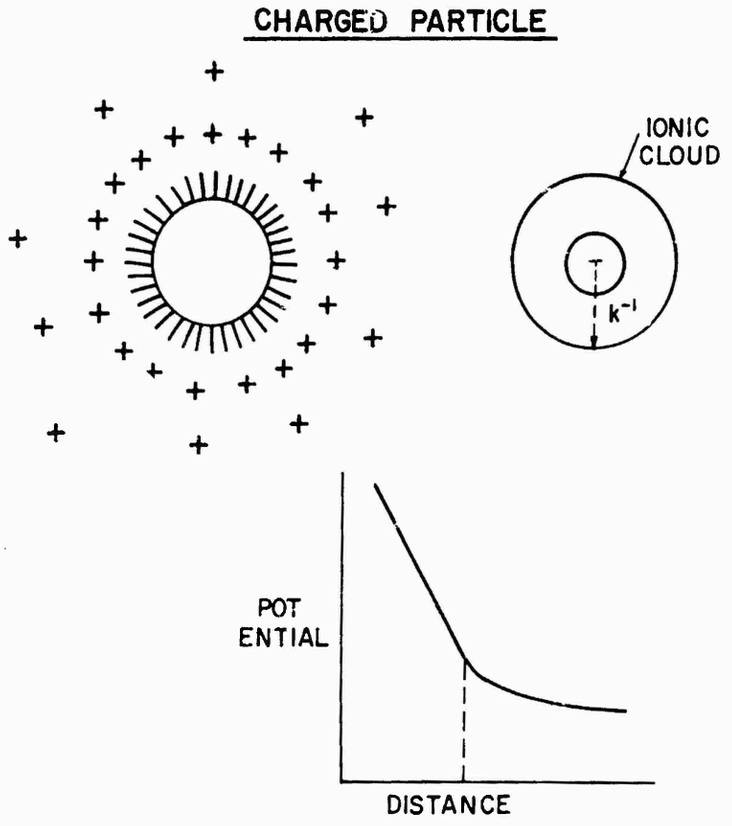

Fig. 1: The double layer and potential gradient surrounding a charged particle.

The Zeta potential can be determined by two main methods: microscopic determination of the velocity of individual particles using the Smoluchovski equation or in the Burton cell where a pure filtrate of solvent is poured on the suspension, a field is applied and the movement of the sharp boundary is monitored [2].

When an electric field is applied to a charged particle it will

move to the electrode with the opposite charge. However, the diffuse double layer around the particle interferes with its movement. The diffuse charge tends to move with the particle to which it is attached but on the other hand it is influenced by the electric field which pulls it in the opposite direction. The particle apparently wins. It moves through the liquid with a diffuse egg-shaped double layer surrounding it (although it is not actually carrying the oppositely charged ionic atmosphere but is rather leaving part of it behind and rebuilding it in front as it moves along). The tendency of the ions in the diffuse d.l. to move in the direction opposite to the movement of the particle has an effect on the velocity. It produces a "drag" which slows down its movement (see Fig. 2) [3]:

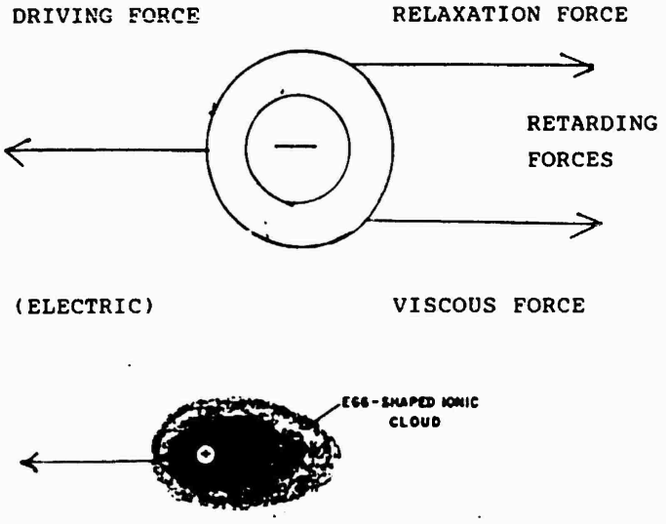

Fig. 2: Egg-shaped ionic cloud and forces acting on a moving particle.

The mobility of the particle is derived by equating the electric force with the frictional resistance and the relaxation force. Thus the mobility μ is given by:

$\mu = E\epsilon\zeta/4\pi\eta\kappa[1+f(kr)]$ where:

μ - mobility
E - field strength
ϵ - dielectric constant of fluid
ζ - zeta potential of particles
η - viscosity of fluid
K - 1/double layer thickness
r - radius of particle

f(kr) varies between 0 and 1 for small and large values of kr respectively.

f(kr) represents the relaxation phenomenon, if k<<<r then:

The Smoluchowski equation is obtained and

$$\mu = (E \cdot \epsilon \cdot \zeta)/4\pi\eta$$

Values of μ vary between $0\text{-}20\times10^{-4}$ cm/sec/1V/cm. The electrophoretic yield is given by:

$$y = a\int \mu ECSdt$$

where C - conc. of particles.
S - area of electrode
t - time

In the above equations it is assumed that the contribution of the hydrodynamic velocity to deposition can be neglected and its importance lies in maintanence of the suspension.
What happens once the particles have reached the electrode? Three theories exist on this subject:
One theory assumes that the particles that reach the electrode undergo an electrode reaction which neutralizes them. This will not explain the fact that MgO deposits are obtained on a

polymeric diaphragm located between two electrodes [4].

The second theory states that the particles are brought to the electrode by a field which exerts sufficient force to overcome the repulsion between them allowing them to come close enough for the London-Van der Waals forces of attraction to predominate [5].

According to the Varwey & Overbeek theory [5] the minimal field strength necessary to overcome the repulsion between particles is calculated from the energy of interaction between particles.

The energy of repulsion between two spherical particles V_R is:

$$V_R=\frac{\varepsilon a\zeta^2}{2}\ln(1+e^{\chi H_o}) \qquad \chi=\sqrt{\frac{4\pi e^2\Sigma n_i z_i^2}{\varepsilon kT}}$$

The energy of attraction - V_A is: $\quad p=\frac{2\pi H_o}{\lambda}$

$$V_A=\frac{A\alpha}{12H_o} \qquad \text{if } 0.5<p<\infty \qquad \alpha=\frac{-2.45}{5p}+\frac{2.17}{15p^2}+\ldots$$

$$V=V_R-V_A \qquad \text{if } 0<p<2 \qquad \alpha=\frac{1}{1+1.77p}$$

a - radius of particle.
Ho - distance between surfaces of particles.
χ - 1/distance of the diffuse d.l.
n - No of ions per unit volume.
A - London van der Waals const.
e - electronic charge.
α - finite time of propagation of electromagnetic waves when particle separation is large.
λ - wavelength of intrinsic electronic oscillations of e.

From these equations the field strength, E, necessary to overcome repulsion between particles can be calculated from:

$$E = 2F/3\varepsilon a\zeta$$

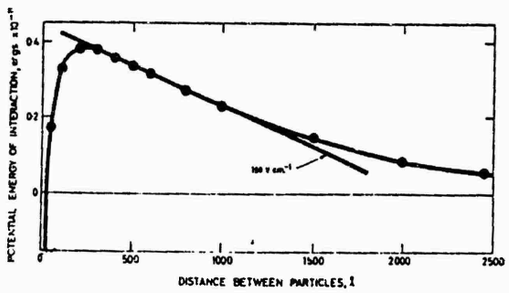

Fig. 3: Energy of interaction between charged particles as function of distance.

A third theory presumes that secondary processes which take place at the electrode can produce ions which coagulate the particles by discharging them or produce hydroxides which polymerize and adsorb on particles holding them together [6].

Parameters which affect electrophoretic deposition are the following:

- Particle charge
- Particle size distribution
- Particle concentration
- Dielectric constant of solvent
- Deposition voltage
- Time

There is an optimum value for the dielectric constant (ϵ). Solvents with too low ϵ do not posses the necessary dissociating power to obtain a charging effect on the particles. Yet too high ϵ leads to high conductivity and low deposition efficiency due to parasitic electrochemical reactions. Thus deposition from an aqueous solution will result in high energy losses and formation of voids due to gas evolution. In previous studies it was found that optimal deposition is obtained in solvents with $\epsilon \cong 14$ [7]. (See Fig. 4

for domain of ε where deposition can be obtained).

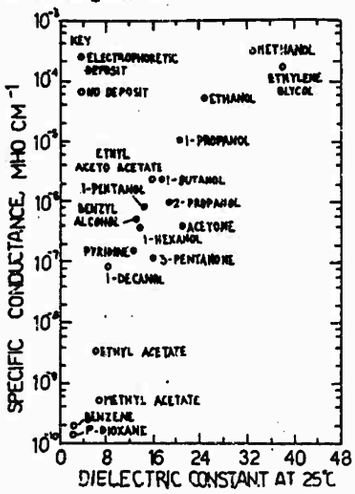

Fig. 4: Dielectric constants of various solvents. Dark dots designate solvents suitable for electrophoretic deposition.

Metal oxide hydrates adsorb H^+ strongly from solution causing positive charging of the colloidal units. This charge is compensated by associated negative charges derived from anions in the solution. The resultant dipole is responsible for the repulsion between neighbouring units [8]. Thus for example:

$$Al(NO_3)_3 + 3NH_4OH \longrightarrow Al(OH)_3 + 3NH_4NO_3$$

$$n\ Al(OH)_3 + X\ HNO_3 \longrightarrow [Al(OH)_3]_n\ XH^+ + XNO_3$$

When silica is placed in water an electric charge develops on it from the transfer of ions between the surface and the liquid phase. The surface charge layer is balanced by ions of an opposite charge in a diffuse layer on the solution side of the interface. The two layers constitute the electric double layer. The ζ potential is a measure of the electrical potential just outside the layer of adsorbed ions that constitute the charge of the surface; the sign of ζ is the sign of the surface charge.

ζ can be measured also by passing a solution under pressure P through a packed bed of particles and measuring E across the bed.

$$\zeta = 4\pi\eta\lambda E/\epsilon P$$

η - viscosity.
λ - specific cond.
ϵ - dielectric constant

Most silicas have a certain population of silanol groups ($\equiv$Si-OH) which can dissociate:

$$\equiv SiOH + OH^- \longrightarrow \equiv(SiO^-) + H_2O$$

Thus a negative charge forms on the surface.

Certain ions such as Al^{3+} can be adsorbed and change the sign of the ζ potential. On top of them citrate ions can be adsorbed to change again to $-\zeta$ [9].
Consecutive transformation of charge is possible such as in the following events [10]:

Silica (neg. charged) + Al^{3+} $\longrightarrow$ positive charge +
citrate ions $\longrightarrow$ neg. charge

Various degrees of hydration are possible. Thus silica particles prepared by precipitation in water or long ageing in it have surfaces entirely covered with $\equiv$SiOH groups. If heated at >400°C the following happens:

$$2\equiv Si\text{-}OH \longrightarrow \begin{matrix} \equiv Si \\ \diagup \\ O \\ \diagdown \\ \equiv Si \end{matrix} + H_2O \text{ (siloxane groups)}$$

At 1200°C only siloxane remains and hydration is slow.

on the solvent. Therefore, the coated electrode must be determined experimentally for each material since the particles acquire the charge spontaneously when mixed with the solvent. Further this charge may be reversed upon addition of ions.

2.2 ELECTROPHORESIS IN POROUS STRUCTURES

In the previous sections the assumption was made that the particle is suspended in an infinite fluid. When electrophoresis in porous structures is considered the presence of rigid boundaries will affect both the electric field and the velocity of the particles.

According to J. Anderson [11,12,13] the pore wall produces three effects on the particle velocity:

- The applied electric field exerts a force on the d.l. of the pore wall if the wall is charged (ζ_w). An electrosmotic flow of the fluid is thus produced which either augments or opposes the electrophoretic velocity of the particle depending on the polarity of ζ_w vs. ζ_p.
- The pore wall distorts the electric flux (current lines) around the particle thereby intensifying the local electric field so that the particle velocity is enhanced.
- The pore wall creates additional viscous stresses in the fluid which retard the particle velocity.

Anderson analyzed the effect of the presence of a pore when the particle is located in the centerline of a long pore. Particle interaction is neglected. Two geometries are considered: a cylindrical one $X=a/R$ a - particle radius, (R - pore radius) and a slit $x=a/B$ (B - half width).
The basic equations which apply to this system are:

$\nabla \cdot E=0$ (conservation of charge)

$\eta \nabla^2 V-\nabla p=0$ (Stokes eq., velocity dominated by viscous stresses).

$\nabla \cdot V=0$ (conservation of mass)

Solving these equations one obtains:

$$U_p=[1-1.2899\lambda^3+1.8963\lambda^5-1.0278X^6+0(\lambda^8)]x\frac{\varepsilon(\zeta_p-\zeta_w)E_\infty}{4\pi\eta}$$

for a cylinderical configuration, and:

$$U_p=[1-0.2677\lambda^3+0.3383\lambda^5-0.0402\lambda^6+0(\lambda^8)\cdot\frac{\varepsilon(\zeta_p-\zeta_w)E_\infty}{4\pi\eta}$$

for a slit configuration

It should be noted that the pore size effect enters first at λ^3. Therefore λ has a weak effect. This is because of a fast decay of electrical and velocity disturbances from a particle moving in an unbounded field.

The disturbance to the electric field is given by:

$$E_p=\frac{1}{2}(\frac{a}{r})^3[I-\frac{3\vec{r}\vec{r}}{r^2}]E_\infty$$

$$V_p=-\frac{1}{2}(\frac{a}{r})^3[I-\frac{3\vec{r}\vec{r}}{r^2}]U_0 \qquad U_0=\frac{\varepsilon(\zeta_p-\zeta_w)E_\infty}{4\pi\eta}$$

Both fall off with λ^3.

The pore wall intensifies the electric field moving the particle faster but the effect on the hydrodynamics leads to a larger retardation, thus overall the velocity is reduced as the pore size decreases.

In a closed system the average flow of solution through the porous medium is zero and a macroscopic pressure gradient develops to oppose the electroosmotic flow produced by the electric field. The cross-section available for the particle is $(1-\lambda)^2$ for a cylinder and $(1-\lambda)$ for a slit.

cylinder:

$$U_p=\frac{\varepsilon\zeta_p}{4\pi\eta}E_\infty[1+(\frac{\zeta_w}{\zeta_p})(2\lambda-\frac{7}{3}\lambda^2)-(1-\frac{\zeta_w}{\zeta_p})x1289\lambda^3]$$

slit:

$$U_p=\frac{\varepsilon\zeta_p}{4\pi\eta}E_\infty[1+(\frac{\zeta_w}{\zeta_p})(\lambda-\lambda^2)-(1-\frac{\zeta_w}{\zeta_p})\cdot 0.2677\lambda^3]$$

Here the electrophoretic effect comes in at ³ and is weak while the pressure flow has a contribution dependent on and has therefore a stronger contribution.

It is to be stressed that in the above analysis the pore walls were considered to be non-conductive.

2.3 ELECTROCHEMICAL DEPOSITION OF CERAMIC FILMS

It has recently [14] been described in literature that it is possible to synthesize ceramic films from water soluble ceramic precursors by an electrochemical method. The method is based on cathodic reduction of water or another anion as NO_3^-, to generate OH^-. A secondary reaction between the OH^- and an appropriate metal ion present in the solution can result in formation of the hydroxide and oxide of that metal. Thus, Switzer [14] has synthesized CeO_2 in a system where the catholyte was 1.0M cerous ammonium nitrate and the anolyte contained 1.0M $NaNO_3$. The cathodic reactions which took place on a platinum cathode at c.d. of 50mA/cm² were:

$$2H_2O+2e \longrightarrow H_2+2OH^- \quad E_o=-0.83V$$

$$NO_3^-+H_2O+2e \longrightarrow NO_2^-+2OH^- \quad E_o = 0.01V$$

The mechanism of the secondary reaction is not clear yet but it may be:

$$Ce^{4+}+4OH^- \longrightarrow Ce(OH)_4$$

$$Ce(OH)_4-2H_2O \longrightarrow CeO_2$$

The powder deposited on the cathode was identified by X-ray diffraction to be ceric oxide with a cubic lattice constant of 0.5409nm and a crystallite size of 7.0nm. After ultrasonic dispersion the material was found to have a narrow particle size distribution with an average particle size of 1.8μ. The

morphology of the ceramic film will depend mainly on the electric-conductivity of the oxide formed. Thus highly conductive materials can form thick dense films or powders.

It is possible to synthesize oxides by an anodic reaction. This is based on the oxidation of a metal ion to an oxidation state at which it undergoes hydrolysis to an hydroxide or oxide. Switzer [14] has deposited thallic oxide films from a solution of a 0.5M thallous acetate in 1.0M NaOH on silicon substrates. By similar reactions oxides of Ni, Cu, Co,Fe and Mn were deposited by Tend and Warren [15] while Sakai et al. [16] have deposited a mixed Pb-Ti oxide film.

The methods described above differ from the electrophoretic deposition of colloidal ceramic particles. However, we believe that they can become powerful methods for coating flat and complex shapes as well as for impregnation of porous structures with ceramic materials.

2.4 ELECTROCHEMICAL REACTIONS IN POROUS ELECTRODES

Electrochemical reactions in porous electrodes have been studied in two systems mainly:
in fuel cell electrodes and in electrochemical reactors used for processes such as metal ions removal from waste water.

Two groups of electrodes exist: forced flow through and diffusion porous electrodes. Theoretical analysis of reaction kinetics in such systems have been performed by numerous researchers [17,18,19,20].

One of the models used in the analysis of diffusion electrodes is the "straight pore" model (see Fig. 5).

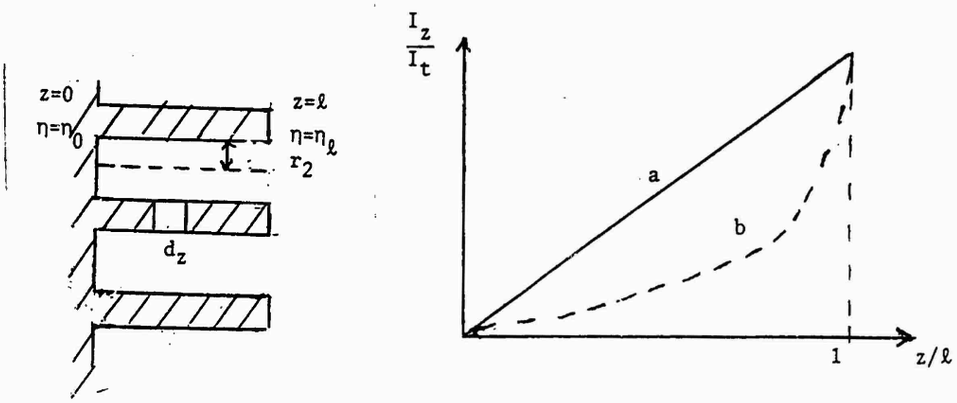

Fig. 5: The straight pore model for diffusion electrodes and the current distribution.

This model assumes that the electrode consists of a number of identical, straight, nonintersecting, cylindrical pores running through the entire length of a conductive matrix.

The basic assumptions in this model are that the pores are filled with electrolyte, no potential drop exists in the solid electrode so that potential gradients are in the solution only, the concentration of reactants is high so that no mass transfer limits exist.

The potential distribution in such a system is:

$$\eta_z - \eta_o = \frac{4RT}{F}$$

The current, up to point Z-I_z, and the total pore current - I_t is:

$$I_z = \tan\left[\frac{a^{\frac{1}{2}}}{2}\right]\left(\frac{y_o}{2}\right)$$

$$I_t = k\pi r_2^2 x \frac{2RT}{\ell F} a^{\frac{1}{2}} \exp\left(\frac{y_o}{2}\right) \tan\left[\left(\frac{a^{\frac{1}{2}}}{2}\right) \exp\left(\frac{y_o}{2}\right)\right]$$

$$k = \frac{1}{\cosh \frac{y_o}{2}} \qquad a = \frac{2i_o \ell^2 F}{K \cdot R \cdot T r_2} \qquad y = \frac{\eta F}{2RT}$$

where

i_o - exchange current
η - overpotential

The current distribution will depend mainly on i_o and k - conductivity of the solution. For $i_o < 10^{-9} A/cm^2$ and $k > 10\ ohm^{-1}cm^{-1}$, there is no potential variation in the pore and the current distribution is linear. If for example $i_o = 10^{-6} A/cm^2$ $k = 0.1\ ohm^{-1}cm^{-1}$ and $r_2 = 5X10^{-4}cm$, then 10% of the current are generated at the first half of the pore when $\eta = 0.3V$. Flow-through porous systems have been analyzed through several models. We shall mention the macroscopic model [18] described in Fig. 6.

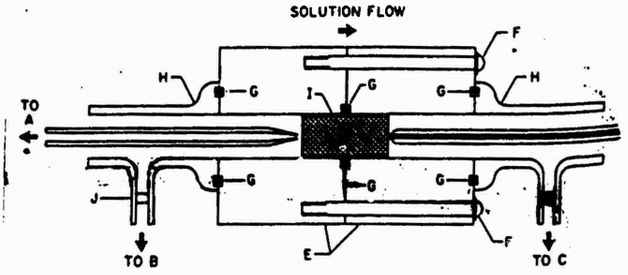

Schematic diagram of cell assembly. A, upstream electrode (SCE); B, counterelectrode; C, downstream reference trode (SCE); D, platinum contact rod (glass-covered); E, Kel body; F, assembly bolt; G, O-ring seal; H, glass tube with joint; I, porous graphite electrode inside heat-shrinkable J, glass frit.

Fig. 6: Flow-through porous reactor.

In this model no detailed description of pore geometry is attempted, the electrode being characterized by the void fraction (ϵ) and the surface per unit volume only (a). The electrode is considered to be isotropic with the matrix condutivity being higher than that of the filled pores so that the potential difference is due to the solution only. The electrolyte flows through the electrode due to a pressure gradient. The potential gradient ($\Delta\Phi_s$) and the collection efficiecy (CE) of the cathodic reduction of metallic ions is given by:

At high flow rates:

$$\frac{\Delta\Phi_s}{I_{max}} \sim \frac{R_s}{2}\frac{p}{U^{2/3}}$$

while at low flow rates:

$$\frac{\Delta\Phi_s}{I_{max}} \sim R_s \frac{U^{2/3}}{p} \qquad \frac{\Delta\Phi_s}{I_{max}} = R_s\{ \frac{U}{ak_mAL}\,[1-\exp(k\frac{-ak_mAL}{U})] -$$

$$-\exp(\frac{-ak_mAL}{U})\ \}$$

where:

a - specific interfacial area

A - cross-section of electrode

km - average mass transfer coeff.

L - length

U - volume flow rate

R_{Ω} - resistance of solution filled pores = L

σ - conductivity of electrolyte

P - pressure gradient

The process of sintering, the compatibility of substrate coating and the evaluation of the oxidation resistance will be discussed in a future report.

CHAPTER 3 - METHODS AND MATERIALS

a) Substrates

Two kinds of substrates were used, a porous graphite and a carbon-carbon composite:

- Porous Graphite UCAR Grade 45
  Porosity - 48%
  Average pore size - 60μ
- 2D Carbon-Carbon (received from Edwards Base, no further details available).

b) Ceramic Materials

Electrophoresis

- Colloidal SiO_2 - Pyrogenic Aerosil
  (submicron 460 m^2/gr)
- Fused SiO_2 (1-40μ)
- Glass Ceramic (borosilicate matrix with SiO_2 and ZrO_2 crystalline phases)
  (ave. size 5-6μ).
- SiC (600 mesh <40μ)
- SiN (0.2-1.0μ).

Electrodeposits

CeO_2, ZrO_2, Al_2O_3 were deposited.

c) Specimens

12-25mm diameter, 5-7mm thick or 20x20x7mm.

d) Deposition parameters

Electrophoresis was carried out from suspensions of

respective particles in non-aqueous solvents. Stirring was applied during deposition. Deposition was carried out at constant voltage with current varying due to deposit formation. Electrodeposition was carried out from aqueous solutions in a two-compartment system with anolyte and catholyte of different compositions. Figs. 7 and 8 describe the experiment set-ups.

Electrophoresis

Deposition voltage - 30-450V
Particle conc. - 3-33 g/l
Solvents - isopropanol, ethanol, hexanol
Temp. - room
Current density - 100-5 mA/cm² (c.d. fell during experiments due to build up of deposit).
Deposition time - for most specimens it was 2 hrs but in cases when thick deposits formed rapidly deposition was stopped when the c.d. fell to 5 mA/cm².
Counter electrodes - stainless steel.
Distance between electrodes - 18mm.

Electrodeposition

Catholytes: 1M Ce $(NO_3)_4$ 1M $Al(NO_3)_3$, 1M $ZrO(NO_3)_2$
Anolyte: 1M $NaNO_3$
Deposition voltage: 5-40V
Current density - 10-50 mA/cm²
Temp. - 25-55°C
Deposition time - 3-120 min
Counter electrode - Pt

Specimen preparation

Ultrasonic cleaning in acetone for 5 min prior to coating and air drying for 24 hrs after deposition prior to examination f deposit. In case of quantitative determination f impregnated SiO_2 the external deposit was removed physica ly.

e) **Testing of deposits**

Specimens were examined in the SEM for morphology. Mapping and line scans were applied for analysis of coating. The SEM used was Jeol T-200.

Examinations were performed on the surface and on cross-sections. The cross-section was obtained by breaking the specimen after removal of the external coating with compressed air. X-ray diffraction was made on the deposits obtained by electro-reduction as received and in some cases after thermal treatment. Quantitative determination of SiO_2 induced into the porous structure of graphite at varying deposition parameters was made by analyzing the SiO_2 residue after burn-off of the carbon at 950°C for 20 hrs. The white residue was treated with HNO_3+HF forming volatile HF_3Si. Weight differences were determined in both stages.

f) **Electroosmotic flow**

This effect was studied on graphite specimens that were cleaned and weighed prior to immersion in isopropanol and water for defined intervals with and without an electric field (50V/cm). The specimens were weighed again after immersion. On basis of weight gain, dimensions and percentage of porosity, the percentage of filled pores was calculated.

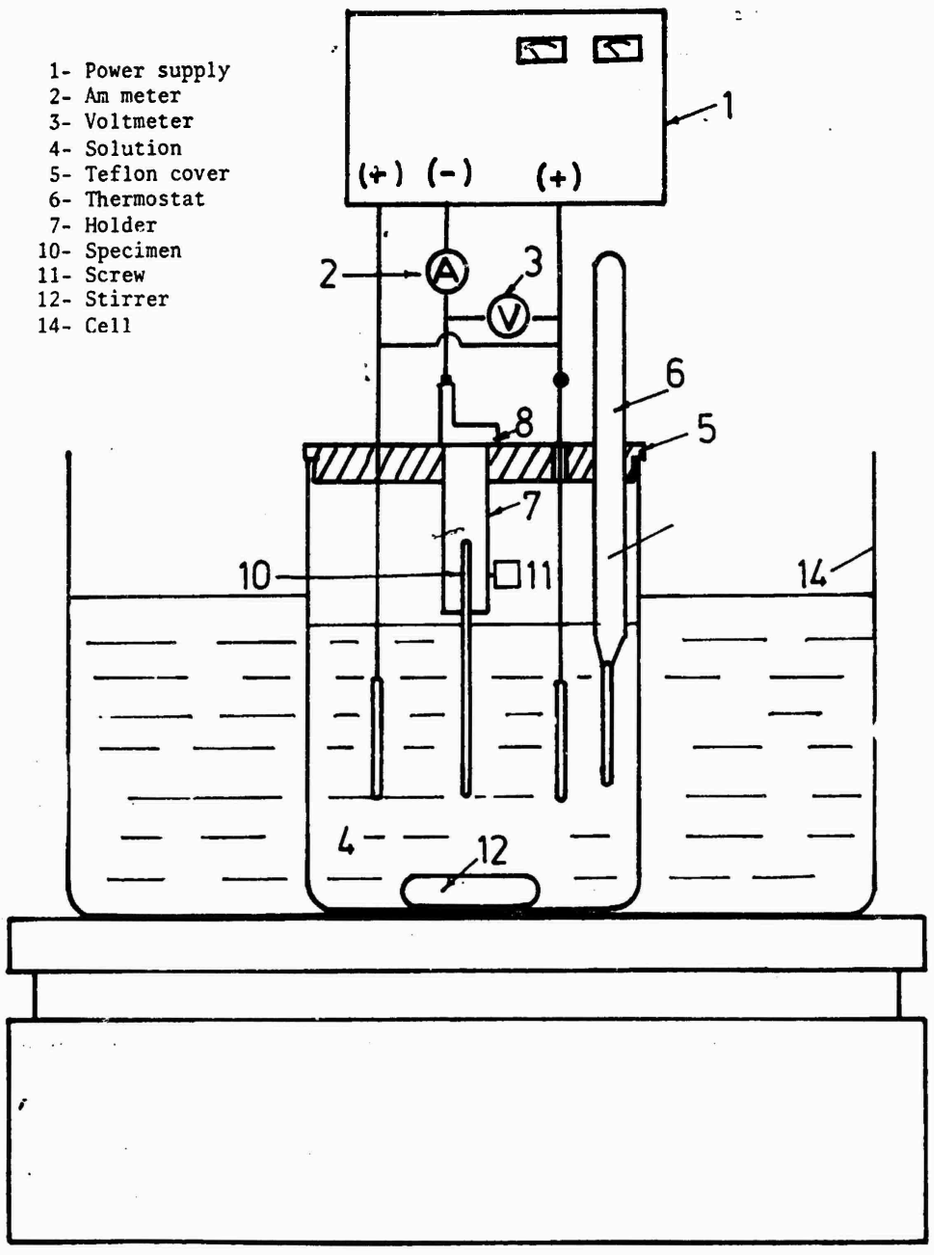

Fig. 7: Experimental set-up for electrophoresis.

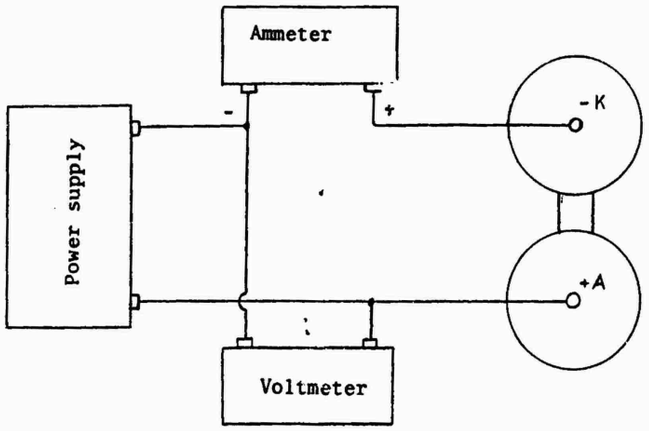

Electrochemical cell:
anodic & cathodic
compartments

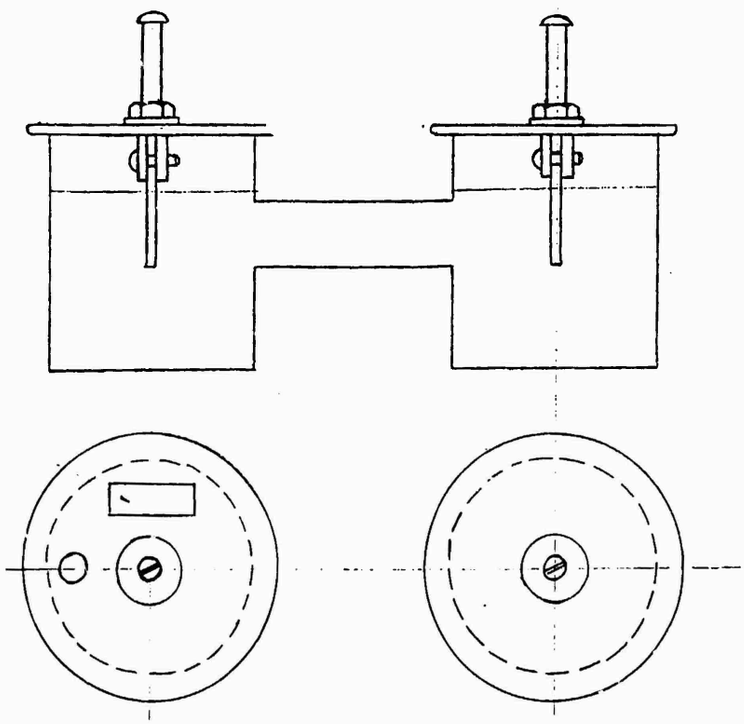

Fig. 8: Experimental set-up for electrodeposition.

CHAPTER 4 - RESULTS

4.1 Electrophoretic deposits

4.1.1 Surface morphology

The surface morphology of the "green" deposits, both on graphite and C-C specimens, was examined by optical and electron microscopy. Figs 9-13 represent the macroscopic view of the various deposits excluding colloidal SiO_2 which resulted in a transparent coating. The surface view of the SiO_2 deposit is seen in SEM micrographs (Figs. 14,15) including a x-ray mapping (Fig. 16).

4.1.2 Morphology and composition of cross-sections

In order to verify the possibility of induction of ceramic particles into the porous substrate cross-sections of coated specimens of graphite and in a few cases of C-C, were prepared (following removal of external coating) and studied in the SEM. At this stage, the study concentrated on the colloidal SiO_2 deposit (Figs. 24-44) with only initial examinations of the SiC, SiN and fused SiO_2 (Figs. 17-23). For the colloidal SiO_2, the cross-sections of specimens obtained under varying deposition parameters were examined at locations differing in distance from surface so as to study the "in depth" distribution of SiO_2. However, only two locations are shown here, one close to the surface (about 0.5mm from surface and termed "edge") and one in the middle of the cross-section (3.5mm from edge termed "center") (see Figs. 29-44). For specimens 8 & 9 no center photo is shown since there was no SiO_2 found. Prior to the systematic study; the existence of SiO_2 in the cross-section was established without specific notice of the distance from surface (Figs. 24-28). The deposition parameters for the colloidal SiO_2 specimen seen in Figs. 29-44 are described in Table 1 . For reference a cross-section of an uncoated graphite specimen was examined also (Fig. 44).

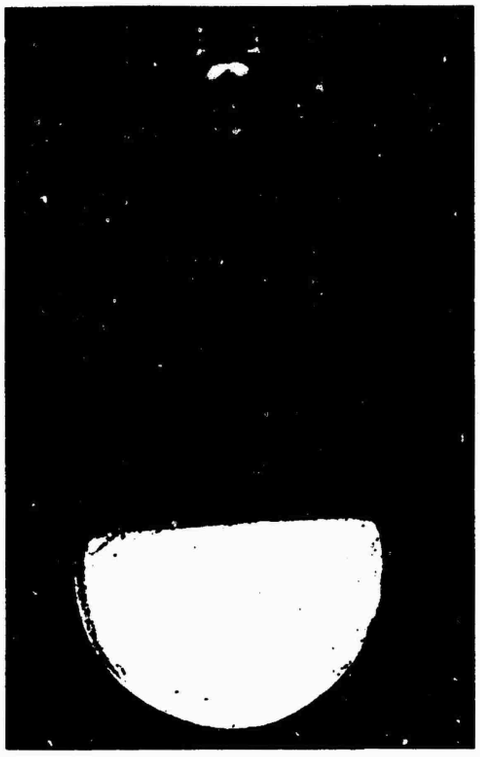

Fig. 9: Glass ceramic on graphite (electrophoresis).

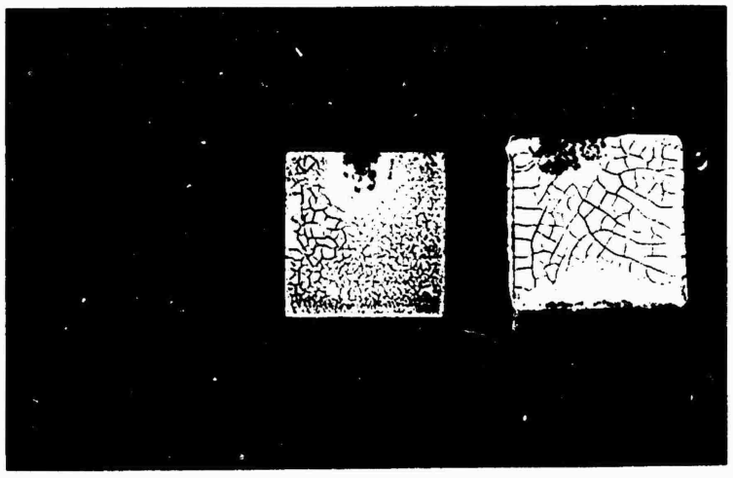

Fig. 10: SiC, SiN and fused SiO_2 on graphite (electrophoresis).

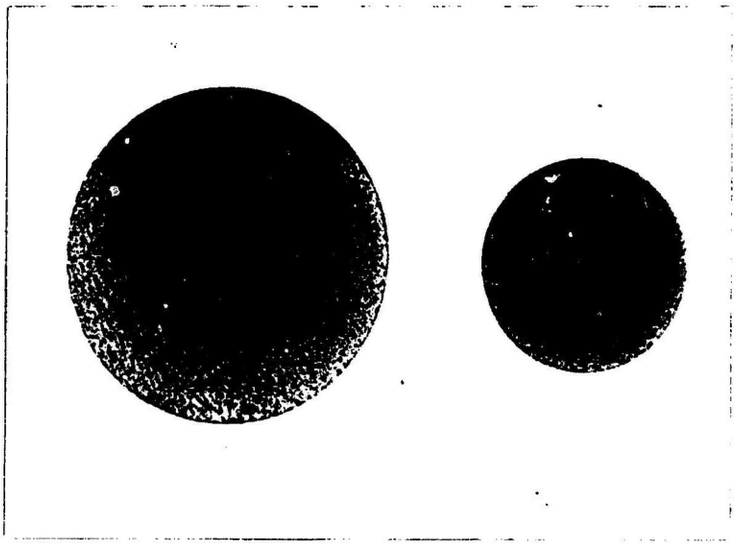

Fig. 11: SiC on C-C composite (left perpendicular direction to fiber cloth, right parallel to cloth) - electrophoresis.

Fig. 12: Fused SiO_2 on C-C composite (left perpendicular, right parallel) - electrophoresis.

Fig. 13: SiN on C-C composite - electrophoresis.

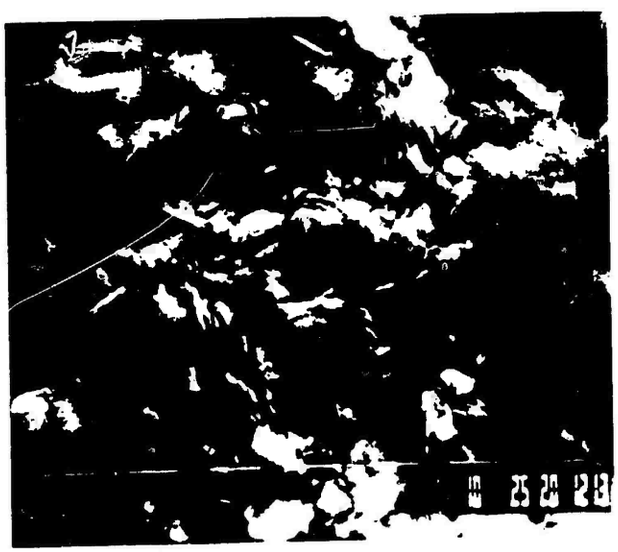

Fig. 14: Colloidal SiO_2 on graphite (electrophoresis).

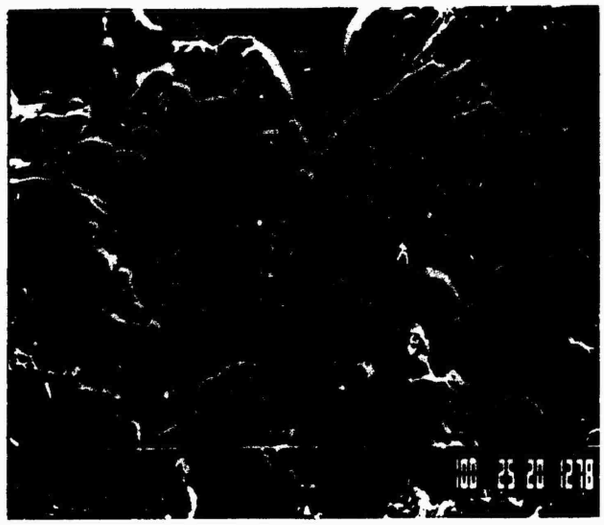

Fig. 15: as in Fig. 14 but another specimen.

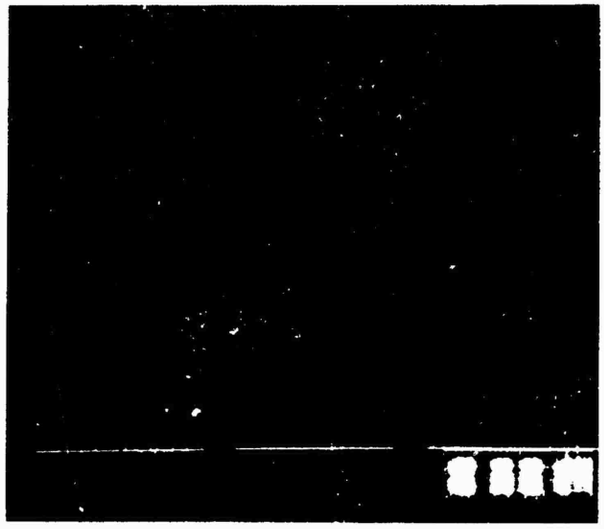

Fig. 16: X-ray mapping of Si on area seen in Fig. 15.

Table 1: Deposition parameters for specimens examined in the SEM (Figs. 29-44) (Deposition time - 2 hrs).

Specimen No.	Solvent	SiO_2 concen. (g/l)	Deposition Voltage (V)
1	Isopropanol	13	30
2	"	"	150
3	"	"	150
4	"	"	300
5*	"	"	300
6	Ethanol	3	30
7	"	"	150
8	"	"	300
9	"	"	450
10	Pentanol	"	30
11	"	"	150
12	"	"	300
13	"	"	450
14	Isopropanol	3 g/l SiN	30
15 Blank	-	-	-

* Exposure to solvent for 5 min prior to deposition.

Fig. 17: Cross-section of graphite specimen coated with fused SiO_2. (Morphology + x-ray mapping of Si).

Fig. 18: Cross-section of graphite specimen coated with SiC.

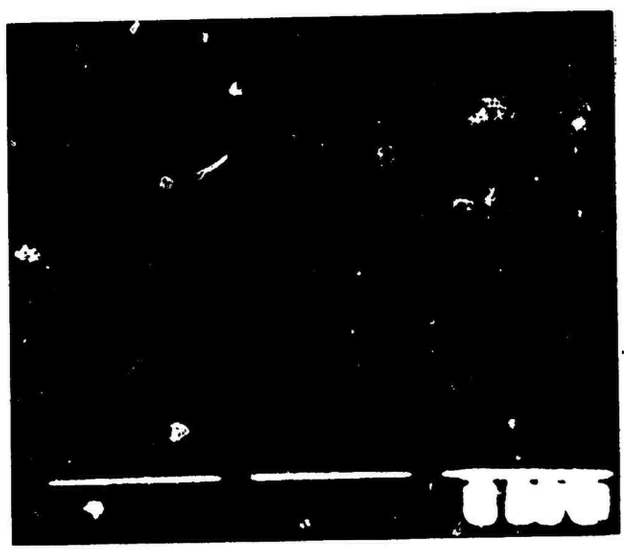

Fig. 19: X-ray mapping of Si on area seen in Fig. 18.

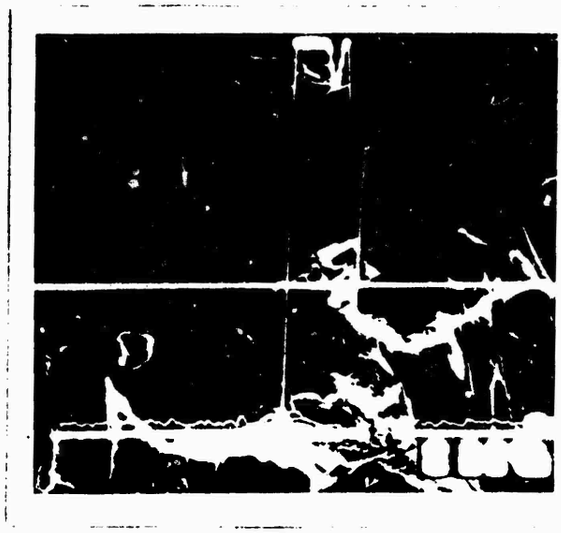

Fig. 20: SiC particle in C-C section.

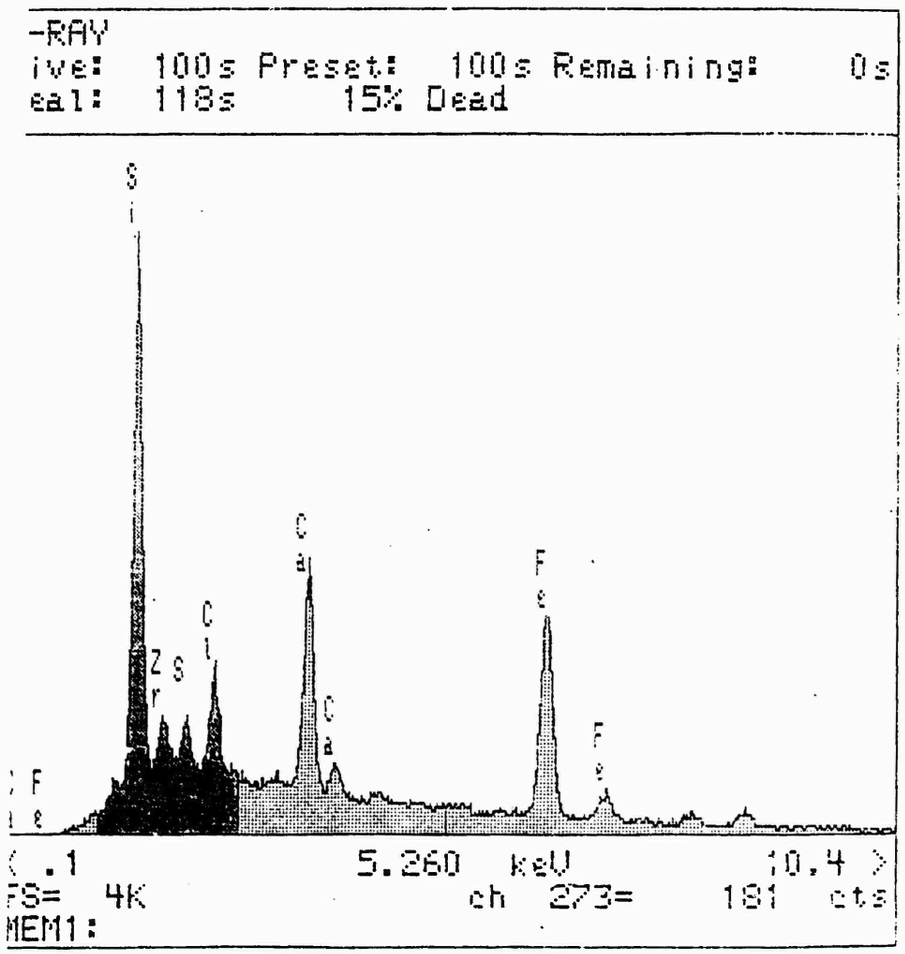

Fig. 21: EDS spectrum of particle seen Fig. 20.

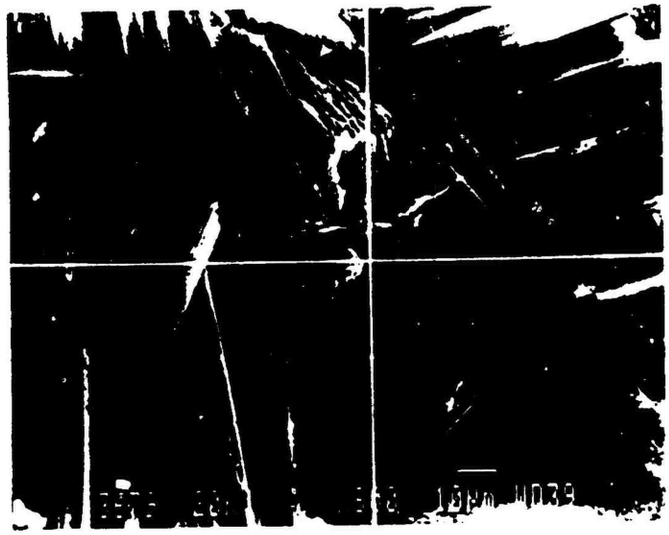

Fig. 22: SiN particle in C-C composite section.

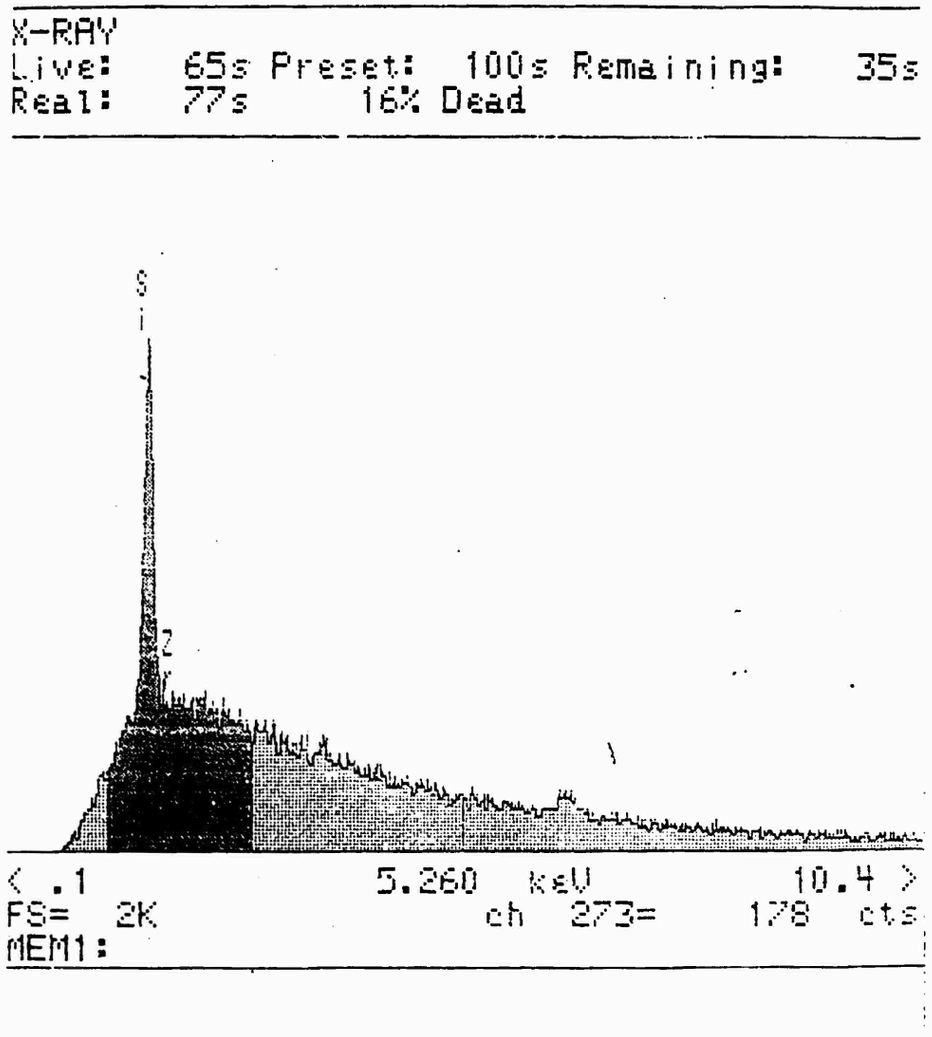

Fig. 23: EDS spectrum of particle seen in Fig. 22.

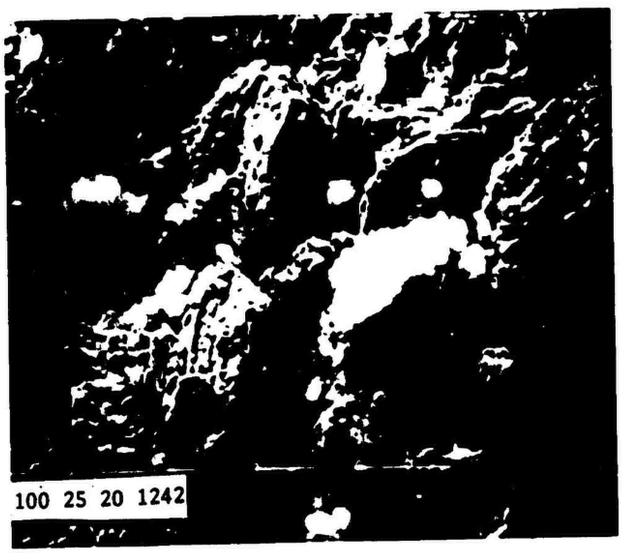

Fig. 24: Cross-section of graphite specimen coated with colloidal SiO_2.

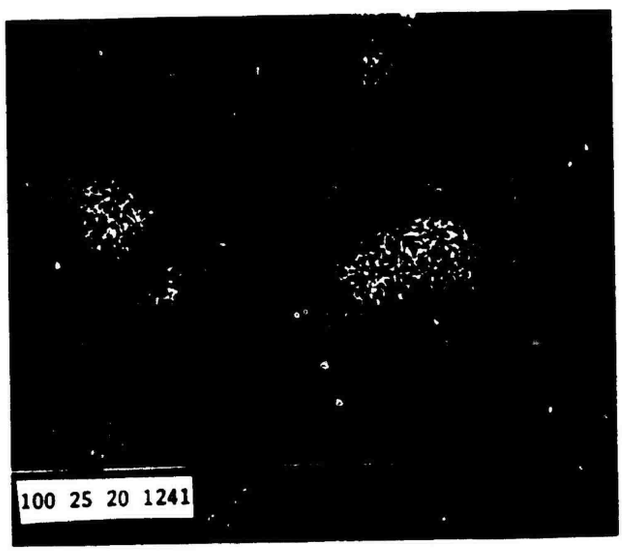

Fig. 25: X-ray mapping for Si on area seen in Fig. 24.

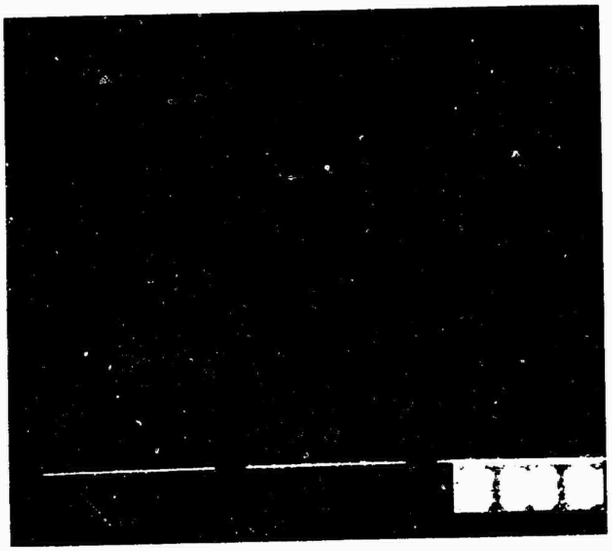

Fig. 26: X-ray mapping for Si on another area seen of cross-section.

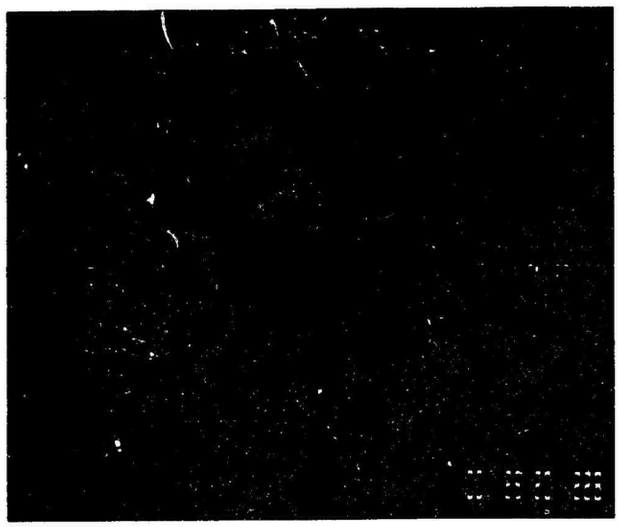

Fig. 27: As in Fig. 24.

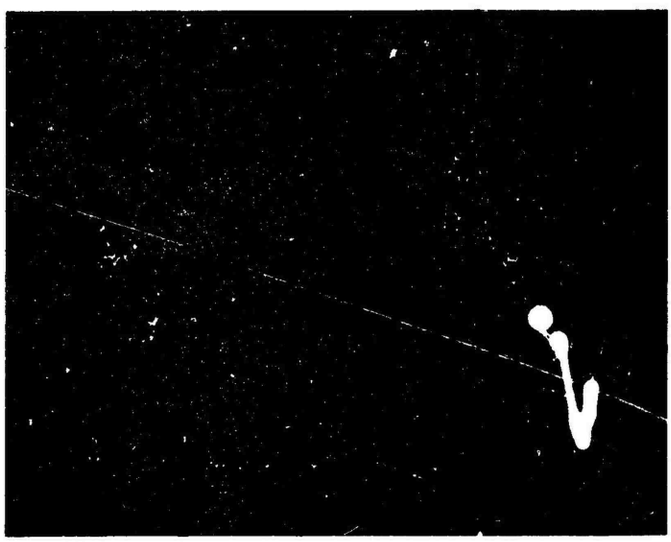

Fig. 28: Line scan for Si along the line seen in Fig. 27.

edge

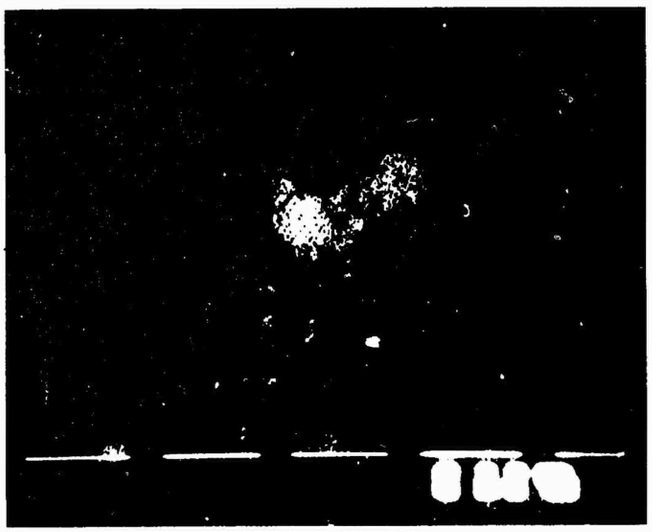

center

Fig. 29: Cross-section of specimen No. 1 - Si mapping.

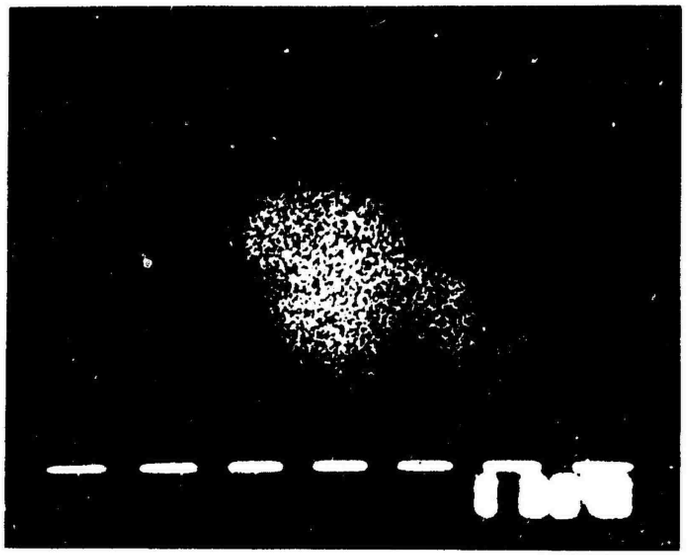

edge

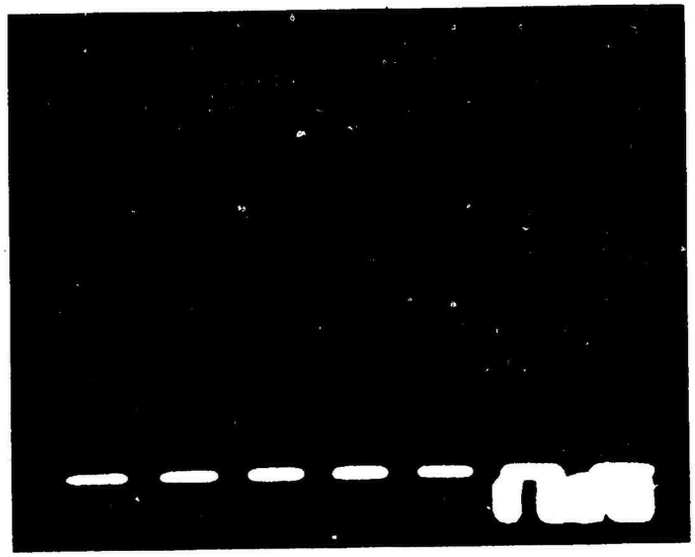

center

Fig. 30: Cross-section of specimen No. 2 - Si mapping.

edge

center

Fig. 31: Cross-section of specimen No. 3 - Si mapping.

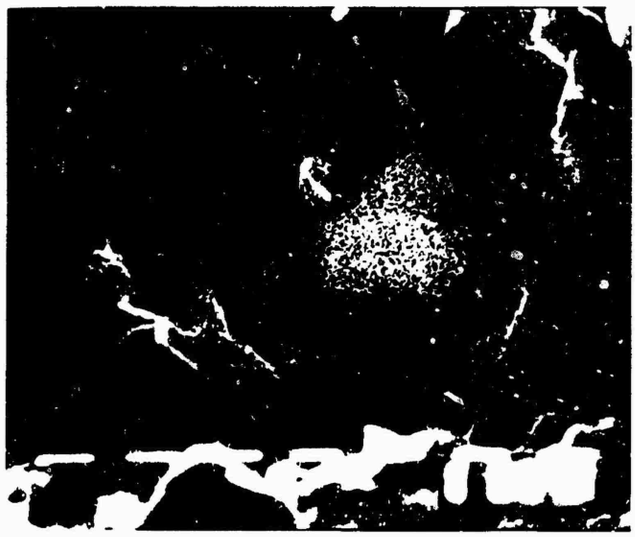

edge

center

Fig. 32: Cross-section of specimen No. 4 - Si mapping.

edge

center

Fig. 33: Cross-section of specimen No. 5 - Si mapping.

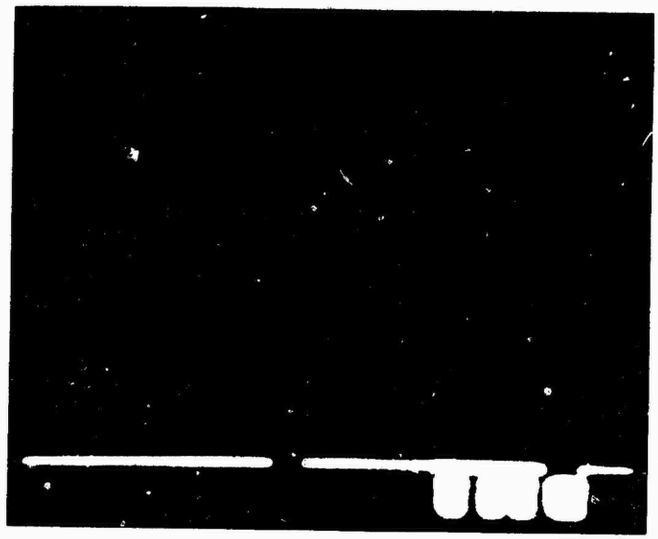

edge

center

Fig. 34: Cross-section of specimen No. 6 - Si mapping.

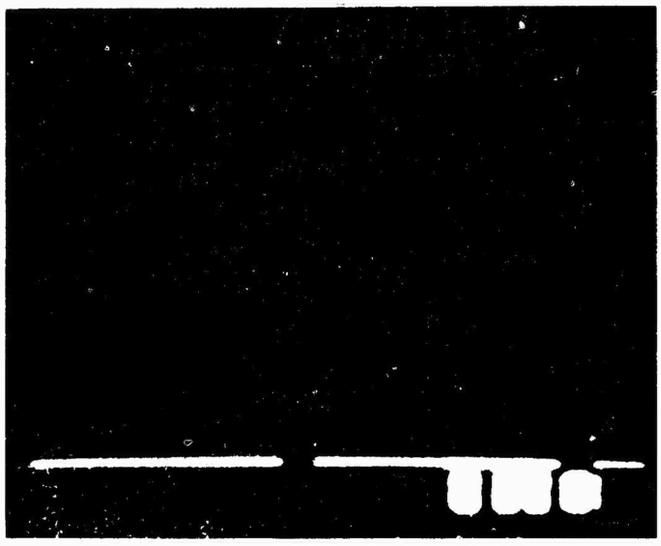

edge

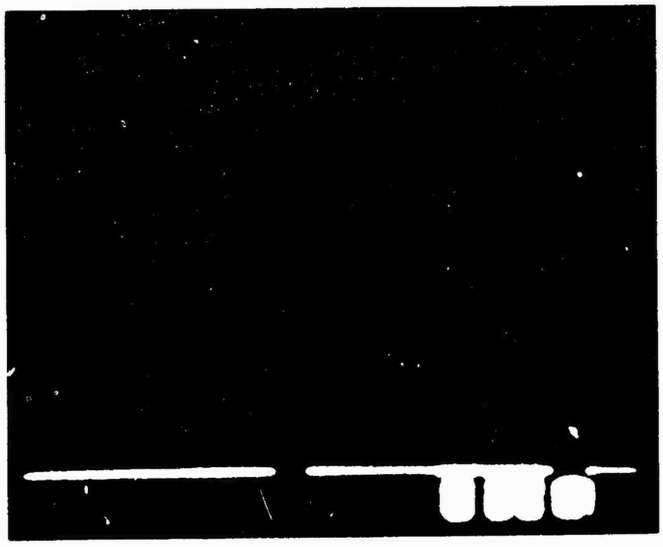

center

Fig. 35: Cross-section of specimen No. 7 - Si mapping.

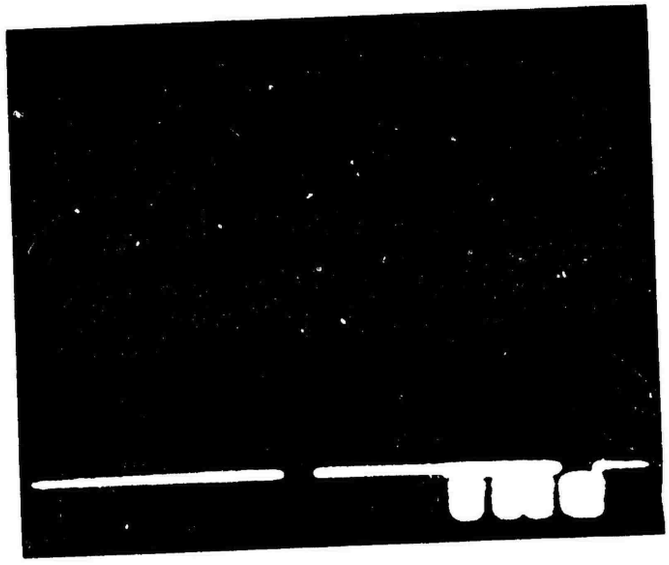

Fig. 36: Cross-section of specimen No. 8 - Si mapping.

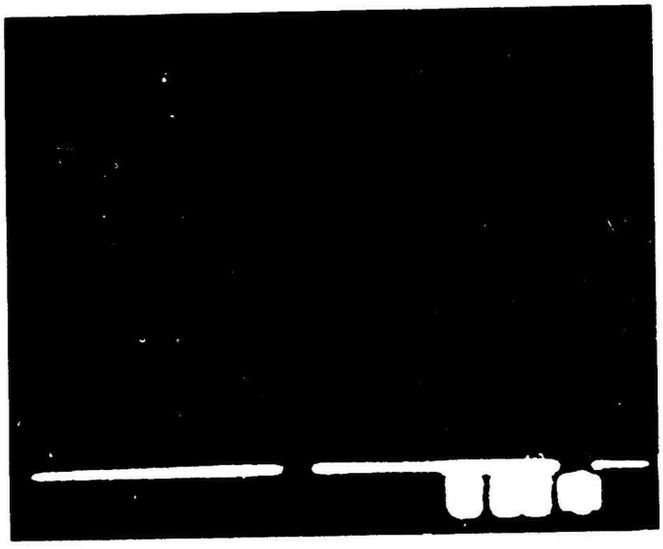

Fig. 37: Cross-section of specimen No. 9 - Si mapping.

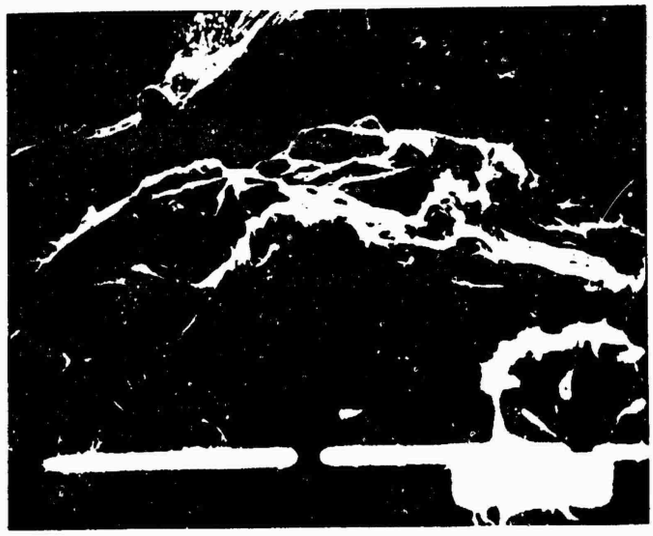

edge

center

Fig. 38: Cross-section of specimen No. 10 - Si mapping.

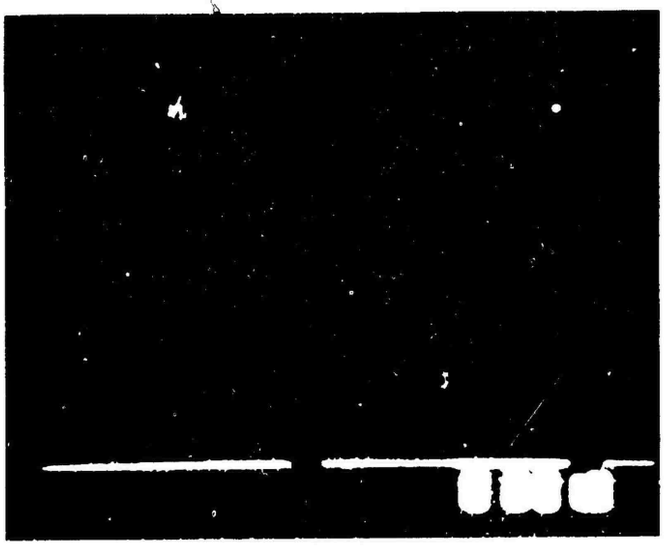

edge

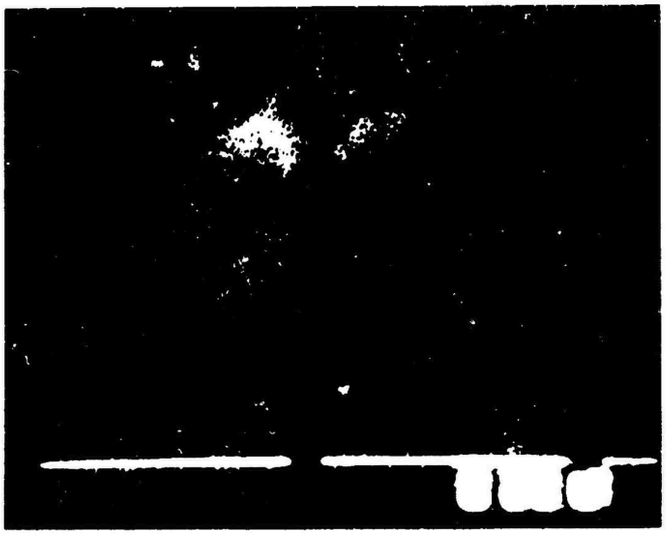

center

Fig. 39: Cross-section of specimen No. 11 - Si mapping.

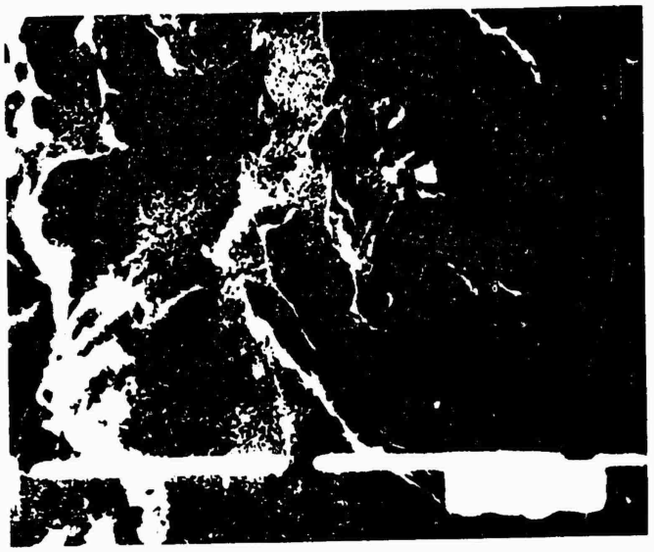

edge

center

Fig. 40: Cross-section of specimen No. 12 - Si mapping.

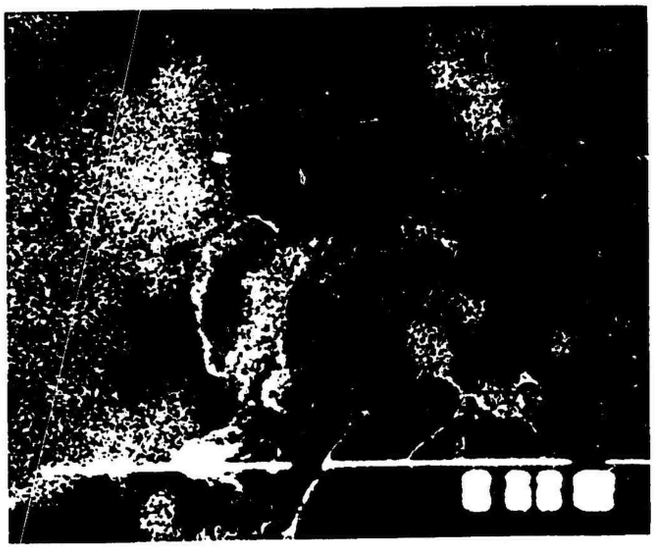

edge

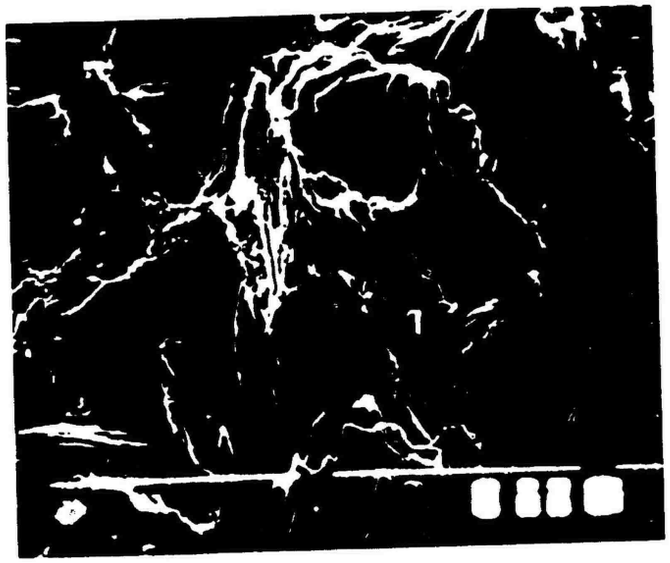

center

Fig. 41: Cross-section of specimen No. 13 - Si mapping.

Fig. 42: Si - line scan of cross-section of specimen 13.

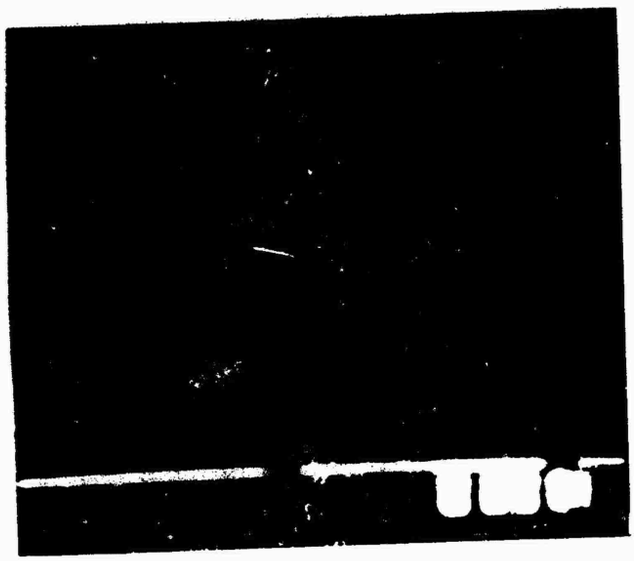

edge

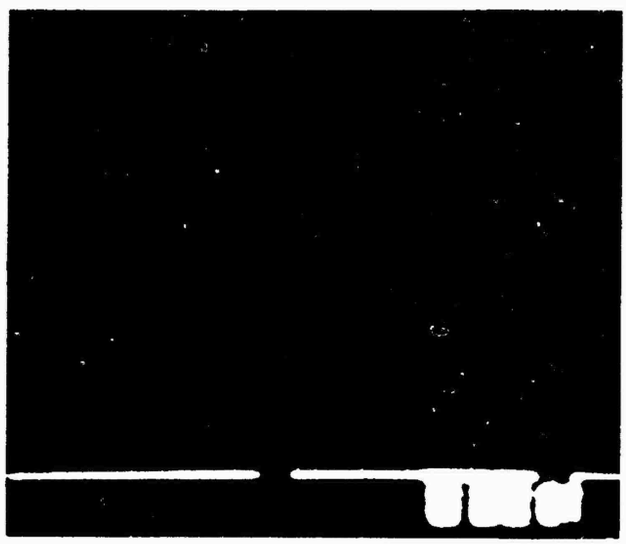

center

Fig. 43: Cross-section of specimen No. 14 - Si mapping.

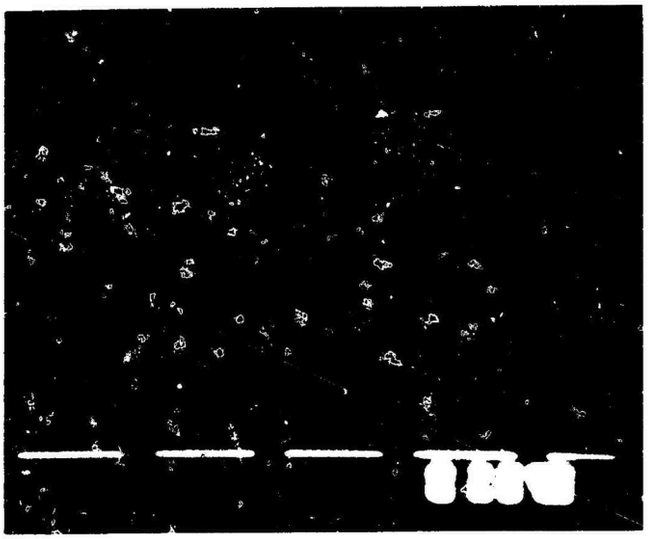

edge

Fig. 44: Cross-section of uncoated specimen - Si mapping.

4.1.3 The electroosmotic effect

According to J. Anderson [11] when a porous medium is brought in contact with a solvent an applied electric field will cause an electroosmotic flow of the solvent into the pores provided the pore walls are charged. To verify the existence of this effect the following experiments were carried out:

Specimens of porous graphite (20x20x7mm) were immersed in distilled water (pH=5.5) and in isopropanol. The weight gain as function of immersion time with and without the existence of an electric field (50V/cm) was determined. Based on pore volume and solvent density the percentage of pores filled was determined (see Table 2 and Fig. 45 next page).

4.1.4 Electrophoretic impregnation of a porous substrate with ceramic particles

The amount of colloidal SiO_2 induced into porous graphite at varying deposition parameters was determined. The determination was performed by analyzing quantitatively the amount of SiO_2 in the specimen after physical removal of the external coating and graphite layer. The analytical method is described in chapter 3. The amount of SiO_2 was expressed in weight percents as related to the graphite specimen. A blank specimen (uncoated) was tested too and a background value of 0.03% was found. Table 3 describes the deposition parameters and results obtained. From these results the dependence of degree of impregnation on deposition voltage, particle concentration and type of solvent was offered and presented in Figs. 46-48.

Table 2: Influence of electric field on pore filling

I-Propanol						Water						Time of Exposure min
Field			No Field			Field			No Field			
Wt-Wo/gr	Wt/gr	Wo/gr	Wt-Wo/gr	Wt/gr	Wo/gr	Wt-Wo/gr	Wt/gr	Wo/gr	Wt-Wo/gr	Wt/gr	Wo/gr	
0.8341 80%	5.3050	4.4709	0.3966 38%	4.8107	4.4141	0.4612 34%	5.0810	4.6198	0.1585 12%	4.8485	4.6900	5
0.8810 84%	5.2963	4.4153	0.7932 75%	5.2583	4.4651	1.071 79%	5.5957	4.5247	0.1585 12%	4.6408	4.4823	15
0.8594 82%	5.3634	4.5040	0.7877 72%	5.2286	4.4409	1.0582 78.9%	5.5897	4.5315	0.1479	4.6295	4.4816	30
			0.7228	5.1349	4.3421				0.1640	4.7800	4.6260	45
			0.8660	5.2982	4.4322				0.1260	4.7766	4.6506	60

Wo - Original weight
Wt - Weight at end of exposure
Results in % - % of pore volume filled.

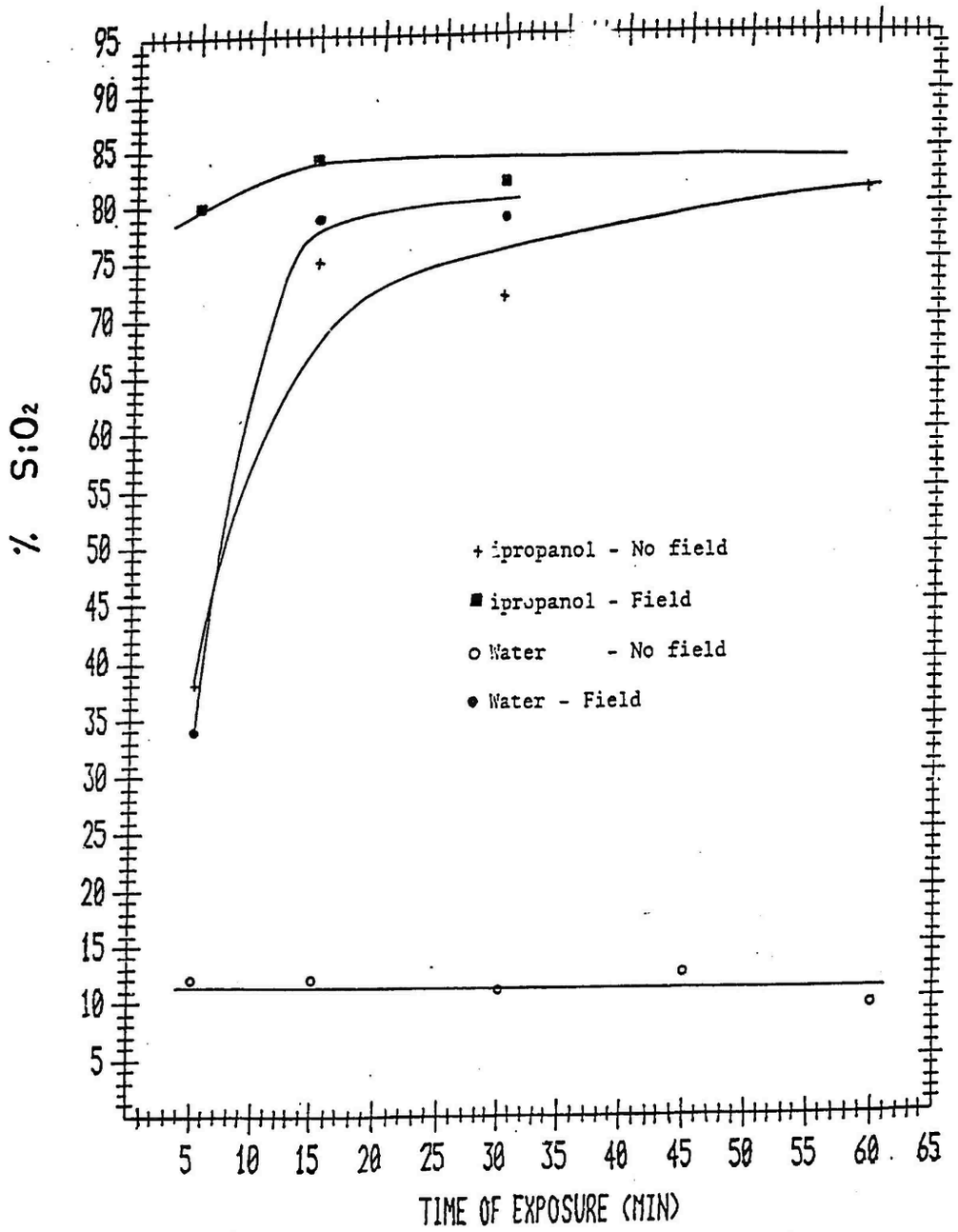

Fig. 45: Percentage pores volume filled as function of exposure time.

Table 3: Weight percentage of SiO_2 in graphite specimens as determined by chemical analysis. (Deposition time - 2 hrs).

Specimen No.	Solvent	Concen. SiO_2 g/l	Deposition voltage (V)	$\%SiO_2$
1	Isopropanol	3	30	0.16
2	"	"	150	0.23
3	"	"	300	0.26
4	"	"	450	0.13
5	"	13	30	0.35
6	"	"	150	0.18
7	"	"	300	0.30
8	"	"	450	0.11
9*	"	"	150	0.61 (wet milling)
10	"	30	30	0.4
11**	"	13	30	0.68
12	Pentanol	3	30	0.1
13	"	"	100	0.1
14	"	"	150	0.2
15	"	"	200	0.1
16	"	13	150	0.1
17	Hexanol	3	150	0.07
Blank				0.03

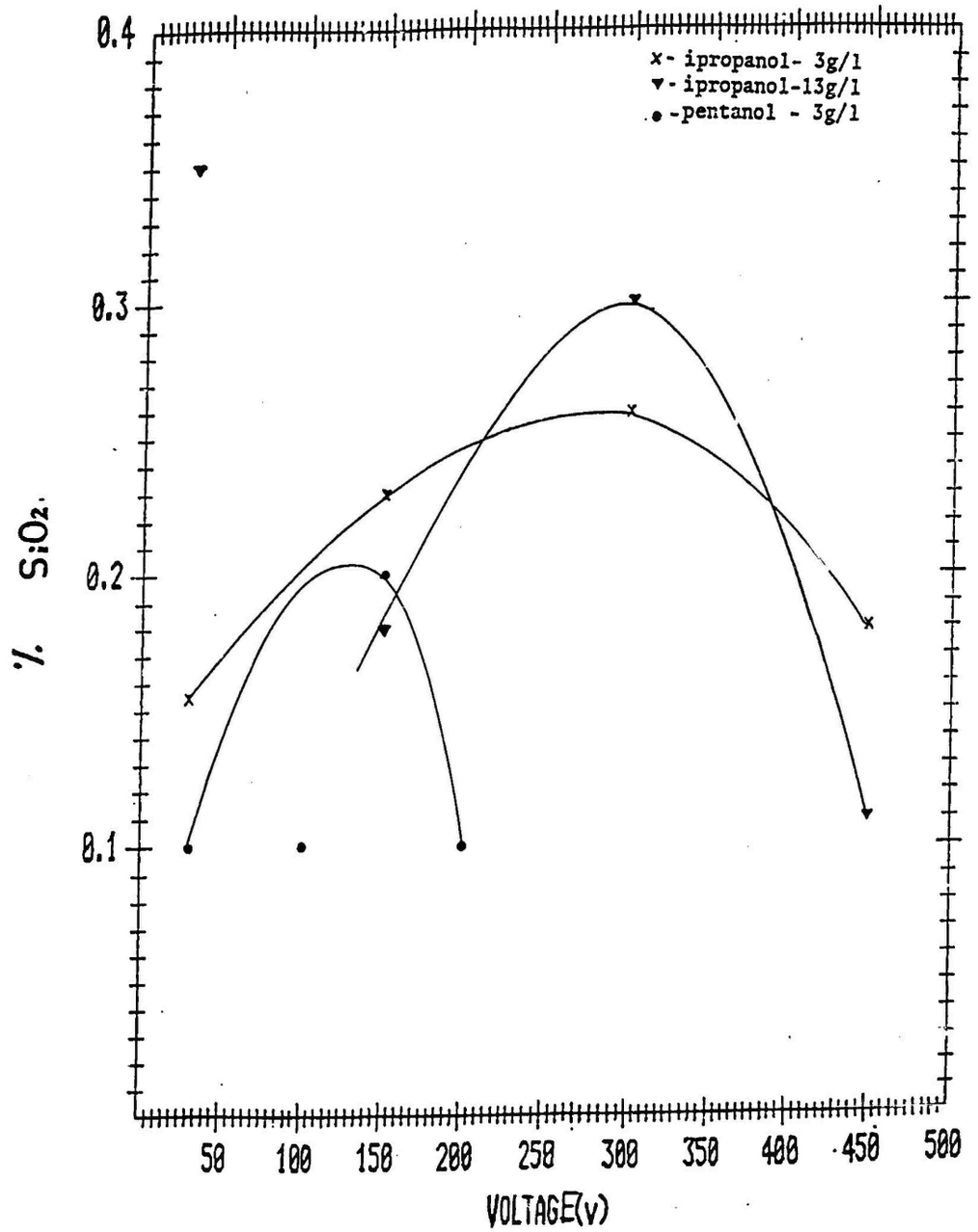

Fig. 46: % SiO_2 induced as function of deposition voltage.

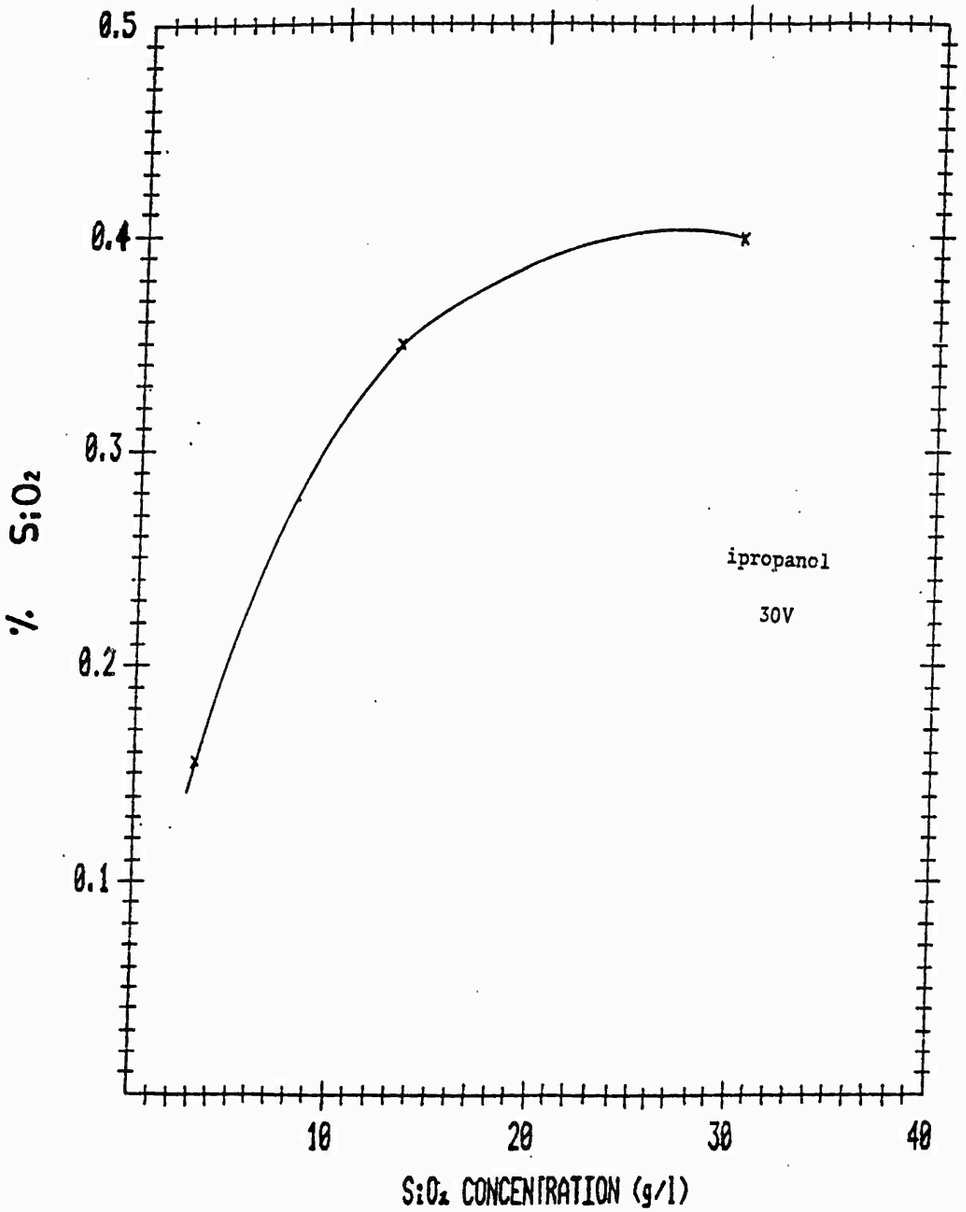

Fig. 47: % SiO_2 induced as function of particle concentration.

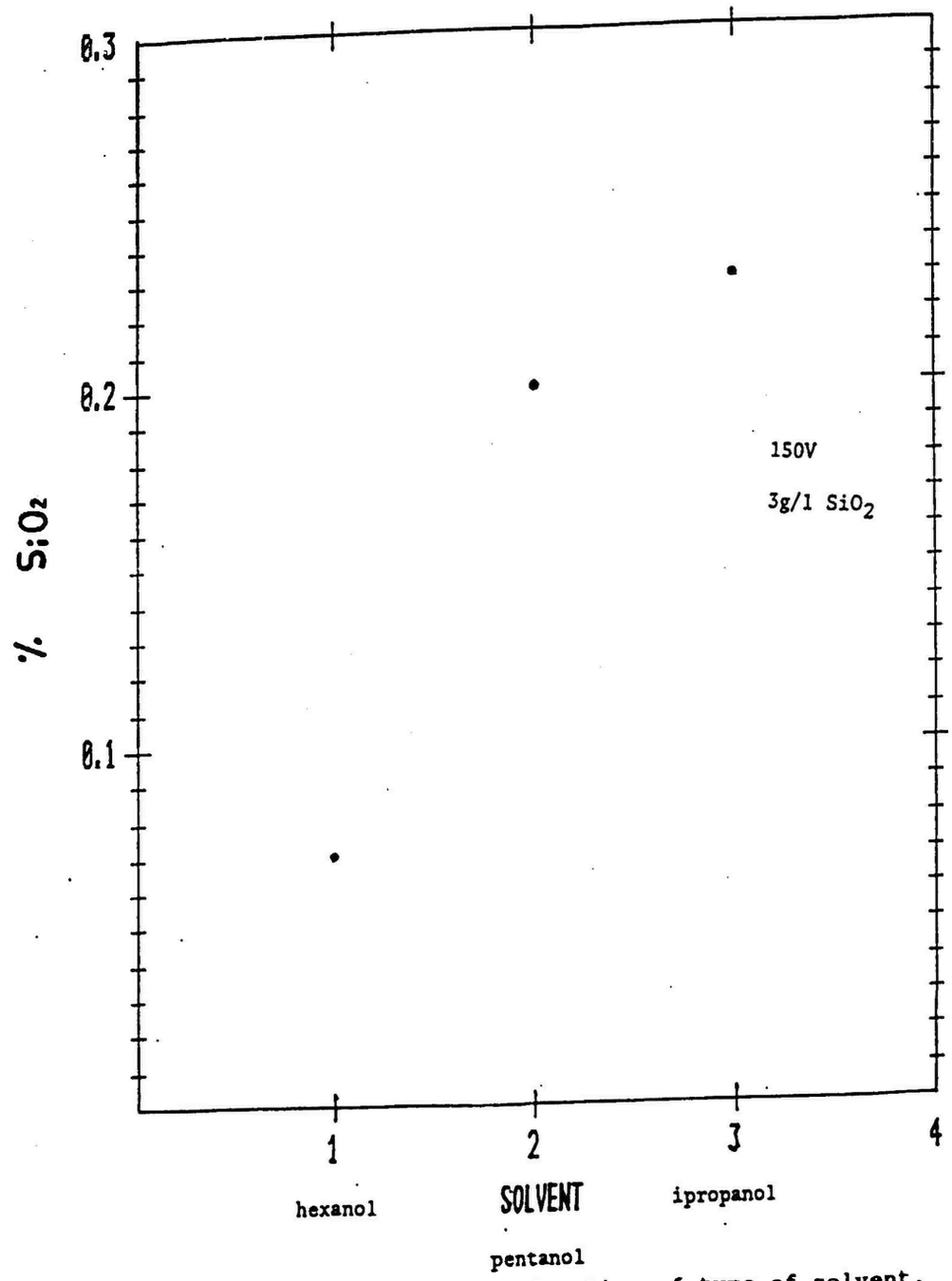

Fig. 48: % SiO_2 induced as function of type of solvent.

4.1.5 Morphology of induced SiO_2

A most interesting phenomenon was observed during the quantitative determination of the SiO_2 induced in porous graphite. As mentioned before, the first stage in the determination is the removal of the graphite by its oxidation at 950°C. In specimens with a higher content of SiO_2 (0.68%), after the carbon volatilization a skeleton of SiO_2 in the exact form and volume of the original graphite specimen was seen (see Figs. 49,50).

4.1.6 Relevant solvent properties

Two solvent properties relavant to electrophoretic deposition are presented in Table 4 based on data from literature. In addition the viscosity of two SiO_2 suspensions in isopropanol and one in pentanol were measured using an Epprecht Rheomat 15 instrument. Measurements of sheer stress as dependent on sheer rate were performed on suspensions which have been stirred for 30 min.

Table 4: solvent properties (at 25°C)

Solvent	Dielectric Constant	SiO_2 conc. g/l	Viscosity (cp)
Ethanol	24.3	-	1.04
Isopro-panol	18.3	-	2
"	-	13	4.37
"	-	30	5.74
Pentanol	13.9	-	3.31
"	-	13	5.21
Hexanol	13.3	-	-

Fig. 49: Induced SiO_2 skeleton remaining after porous graphite volatilization (0.68% SiO_2) specimen in Table 3.

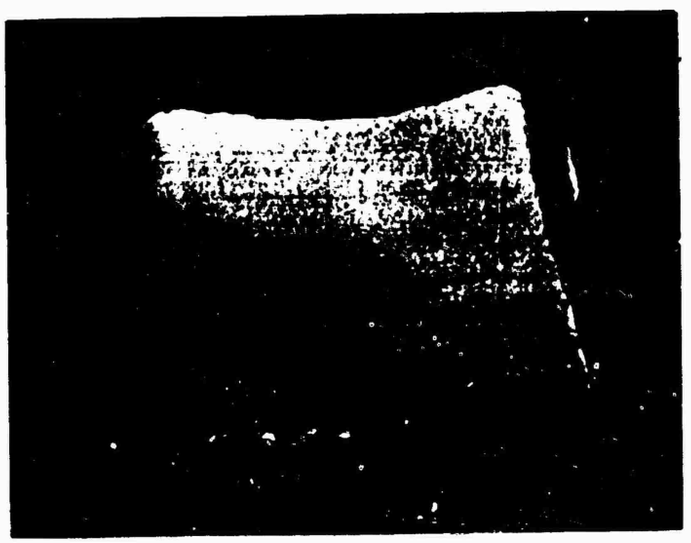

Fig. 50: Cross-section of skeleton seen in Fig. 49.

4.2 Electrodeposition of ceramic films

Three types of oxides (CeO_2, ZrO_2 and Al_2O_3) were deposited from aqueous solutions containing $Ce(NO_3)_4$, $Al(NO_3)_3$ and $ZrO(NO_3)_2$ respectively through an electrochemical reaction. The deposits were formed both on graphite and on C-C specimens which functioned as cathodes in an electrochemical cell.

4.2.1 CeO_2 deposition

The CeO_2 was deposited from a catholyte of 1M $Ce(NO_3)_4$ with an initial pH of 2.2. The anolyte, separated by a glass frit, was 1M $NaNO_3$. The graphite and C-C specimens were cleaned with acetone and then kept in the solution for 20 min in an ultrasonic bath to facilitate penetration of the solution into pores. Surface deposits were obtained at 20V (initial c.d. of 30mA/cm^2) at 30°C for 10 min. In impregnation experiments the voltage and c.d. were lowered (5V, 5 mA/cm^2) and the temperature raised to 55°C. The experiment duration was prolonged too to 30 min. The surface deposit was examined with the SEM and also by X-ray diffraction. Fig. 51 shows the deposit on C-C specimen, while Figs. 52, 53 show the deposit on graphite as seen in the SEM and by mapping of Ce. The results of X-ray diffraction of the deposit and the diffraction of a known CeO_2 powder are given in Table 5.

The formation of CeO_2 deposits inside the matrix of a C-C specimen is shown in Figs. 54-56.

Fig. 51: CeO_2 on C-C composite (electrodeposition).

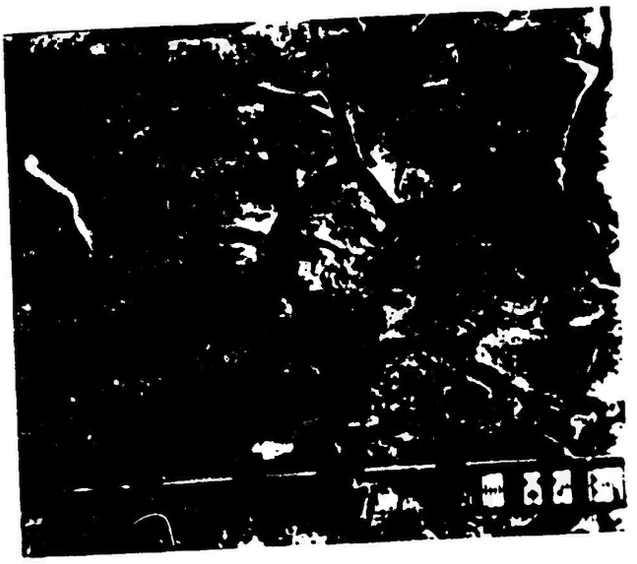

Fig. 52: CeO_2 on graphite (electrodeposition).

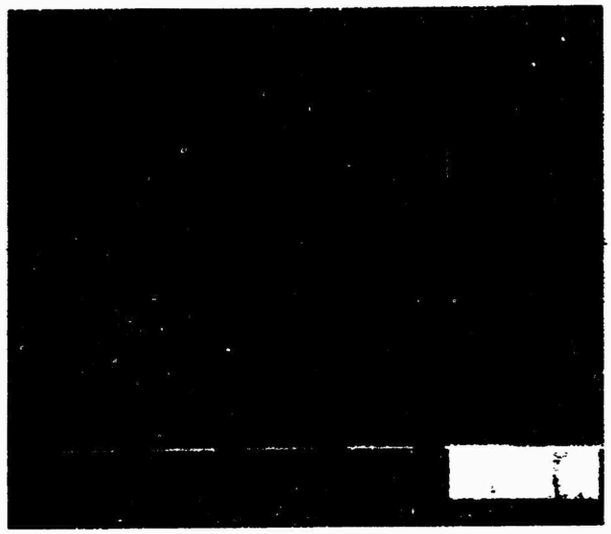

Fig. 53: X-ray mapping of Ce on area seen in Fig. 52.

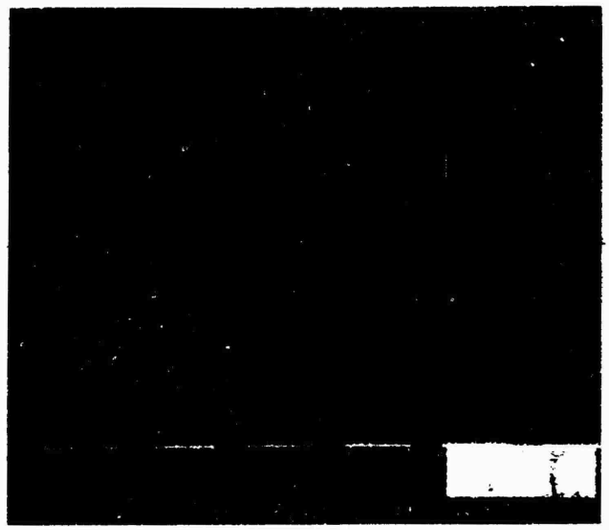

Fig. 53: X-ray mapping of Ce on area seen in Fig. 52.

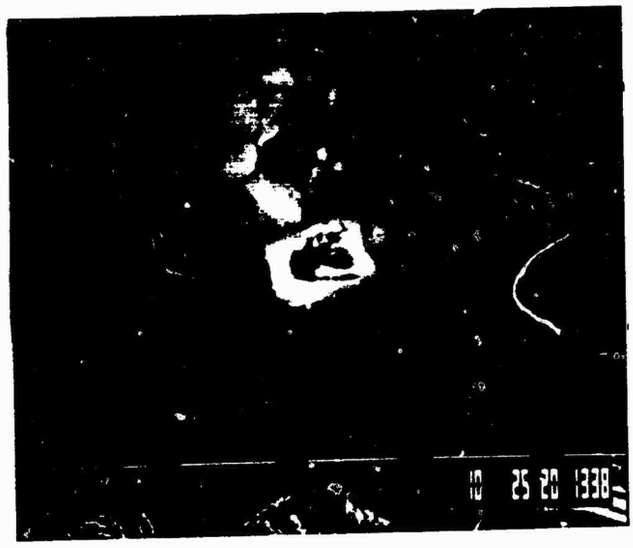

Fig. 55: Like Fig. 54.

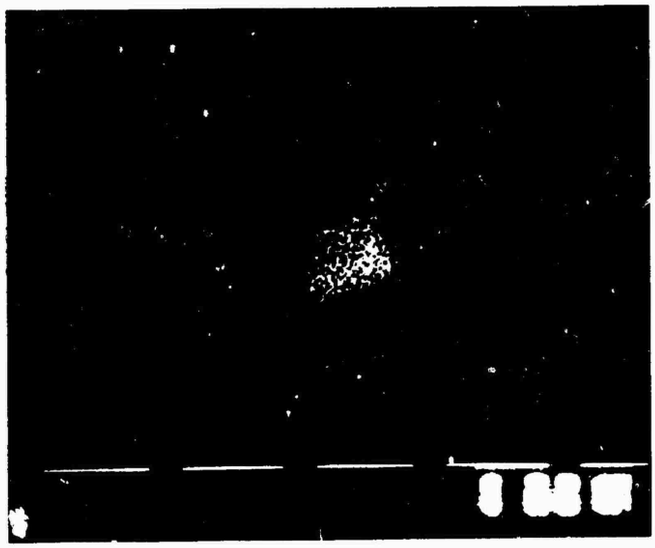

Fig. 56: X-ray mapping of Ce on area seen in Fig. 55.

4.2.2 ZrO_2 deposition

The ZrO_2 deposit was obtained from a solution of 1M $ZrO(NO_3)_2 \cdot 4H_2O$ in the cathodic section and an anolyte of 1M $NaNO_3$. The deposit was obtained on a graphite cathode with a platinum foil acting as the anode. The deposition was performed at a constant c.d. of 25 mA/cm² (nominal) which corresponded to a voltage of 5V. The initial pH of the solution was 1.1. Deposition time was 60 min. At the end of the experiment a thin white deposit was evenly distributed on the surface of the graphite. Fig. 57 shows the surface deposit, while Fig. 58 shows the x-ray mapping of Zr on the same area. At a smaller magnification relatively large crystals are seen (see Fig. 59) in some locations. A cross-section through the coated specimen was prepared (by cutting with a diamond saw) and is seen at 2 magnifications in Fig. 60. Microanalysis of the deposit was performed in locations of smaller and larger crystallytes and the results, corresponding to the atomic ratio in ZrO_2 are shown in Figs. 61. X-ray diffraction of the deposit as received indicates an amorphic structure. Further experiments at higher c.ds. and duration showed the possibility to obtain heavy and thick deposits. Calcination experiments are underway and they indicate a crystallization process of the deposit (detailed results will be reported at a later stage).

Fig. 57: ZrO_2 on graphite (electrodeposition).

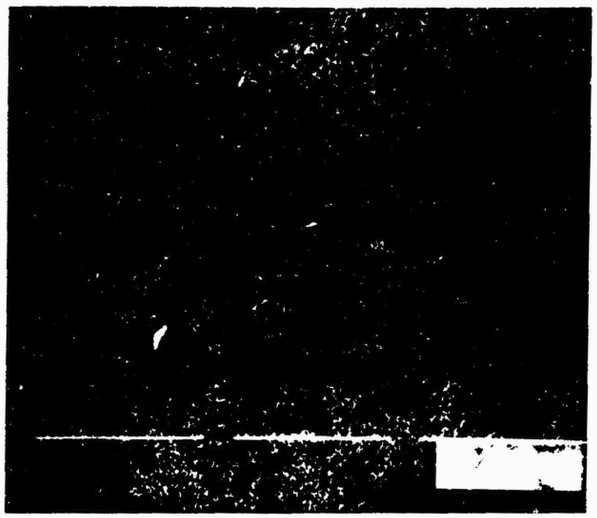

Fig. 58: X-ray mapping of Zr on area seen in Fig. 57.

4.2.3 Al_2O_3 deposition

The possibility to obtain thin white aluminum oxide deposits on graphite was demonstrated in experiments performed with 1M$Al(NO_3)_3$ as catholyte and 1M $NaNO_3$ as anolyte at a c.d. of 50mA/cm² corresponding to 30V for 15 min. Initial pH=2.6. Fig. 62 shows a general view of the deposit on graphite specimen and Figs. 63.64 show a microscopic view and a x-ray mapping of Al of the same deposit.

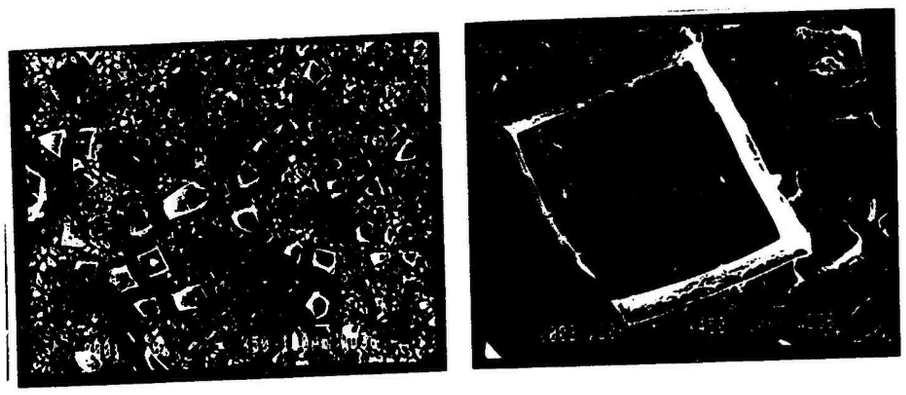

Fig. 59: ZrO_2 on graphite.

Fig. 60: Cross-section through ZrO_2 deposit.

```
                                        LIVETIME(spec.)=   100
 ENERGY     RES      AREA
-  5.7   106.61     65709
TOTAL AREA=    198051
......
Peak at   1.02 keV omitted?
Peak at  15.74 keV omitted?
Peak at  17.64 keV omitted?
FIT INDEX= 2.50

ELMT       APP.CONC    ERROR(WT%)
ZrL : 1    55.260        .411
CaK : 1      .793        .074
..C 2 ZAF'S3

20.00 kV  TILT=  .00 ELEV=40.00 AZIM=  .00 COSINE=1.000

Spectrum:

Last elmt by STOICH.,NORMALISED

ELMT       ZAF    %ELMT    ATOM.%          %OXIDE     FORMULA
ZrL : 1   .919   73.083   32.789   Zr102   98.720       .992
CaK : 1   .904    1.067    1.089   Ca201    1.280       .033
O K : 0   .000   25.850   66.122                       2.000
TOTAL           100.000  100.000          100.000      1.025
```

Fig. 61: Microanalysis of ZrO_2 deposit.

Fig. 62: Al_2O_3 on graphite (electrodeposition).

Fig. 63: Al_2O_3 graphite (electrodeposition).

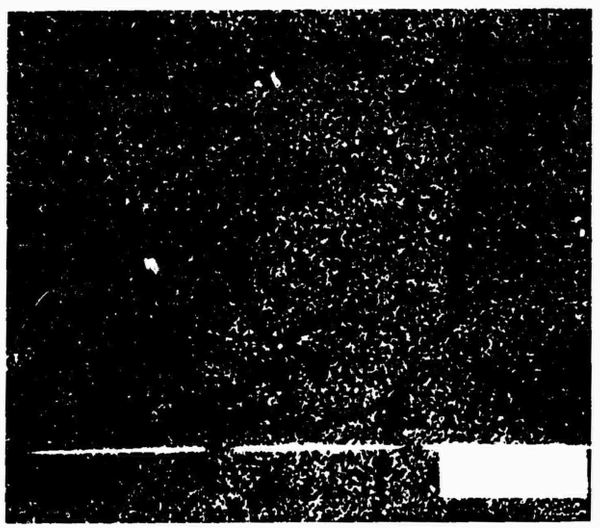

Fig. 64: X-ray mapping of Al on area seen in Fig. 63.

CHAPTER 5 - DISCUSSION OF RESULTS

Surface deposits of all the ceramic materials studied (colloidal and fused SiO_2, SiC and SiN) were obtained both on graphite and C-C substrates by electrophoresis. SiO_2 and SiC deposits formed on the anode indicating the presence of a negative charge on the particles, while SiN deposited on the cathode. The charging mechanism of SiO_2 takes place as indicated in literature, by the ionization of silanol groups present on the surface of silica which has been in contact with water for prolonged periods.

$$\equiv Si\text{-}OH + OH^- \longrightarrow \equiv SiO^- + H_2O$$

The charging of SiC and SiN can be envisaged through an adsorption mechanism with SiC adsorbing negative ions and SiN adsorbing positive ones. In the systems we studied the available ions are OH^- and H^+ deriving from small concentrations of water present in the solvent. The dielectric constant of the solvent (isopropanol) is at an appropriate level so as to enable charging of the particles and yet to prevent electrochemical decomposition of the fluid and evolution of gas.
Under the influence of the electric field the particles move to the electrode with the opposite charge forming a relatively dense and adherent "green coating" the thickness of which depends on the deposition time (Figs. 9-13).

In thick coatings cracking is evident in the green state. This has been encountered in previous work and eliminated by increase of particle surface energy. In the coatings on the C-C composite, a non-uniformity in coverage is observed due to the texture of the carbon fiber cloth and local variations in conductivity (Figs. 11,12). All together the composite is, as expected, sufficiently conductive electronically so as to enable its functioning as an electrode in the electrochemical system.

In addition to the formation of surface deposits, the induction of the particles into the pores of a porous substrate was demonstrated both qualitatively and quantitatively. The qualitative studies were performed on cross-sections of coated

porous graphite in the SEM. Clusters of colloidal SiO_2 are seen inside the cross-sectional (Fig. 24) while in the case of larger particles and as in the case of SiC and fused SiO_2 single discrete particles are seen in graphite (Figs. 17,18) and in C-C (Fig. 20). X-ray mappings of the exposed cross-sections for the Si showed the presence of this element in the clusters and particles. A line scan for Si (Fig. 28) showed variations in its concentration indicating its localization in the induced particles. In some cases the presence of Si in the particle was shown by obtaining its spectrum with peaks characteristic of Si (Fig. 21).

In order to evaluate the degree of penetration of the ceramic particles as function of depth, locations at varying distance from the surface were mapped for Si. This was done for colloidal SiO_2 deposits. Only two locations are shown in this report, one close to the surface and one in the center of the cross-section (Figs. 29-44).

It is very difficult to deduce comparative evaluations from these experiments. Those are much more rigorously obtained from following quantitative determinations of SiO_2. However, one trend is quite clear: the decrease in SiO_2 concentration with depth of specimens.

Quantitative evaluation of the amount of SiO_2 induced into the pores was made by determining the amount of SiO_2 in the porous specimen after removal of the external deposit. Since no sintering of the SiO_2 was performed, it was possible to remove the graphite completely by its gasification at 950°C. The value obtained for SiO_2 in a blank graphite specimen was only 0.03%. The tests were performed for deposits obtained in three solvents at varying deposition voltages and particle concentrations. The choice of solvents was based on their dielectric constant and viscosity. We decided to test in addition to isoproponol a solvent with higher dielectric constant and lower viscosity - ethanol, and two with lower ϵ but higher viscosity - pentanol and hexanol (see table 4). A lower viscosity is expected to facilitate particle penetration due to reduction in viscous

stresses. Powers [7] claims that electrophoretic deposition is obtainable only in a definite range of dielectric constants (d.c.) (ϵ=12-25). It was of interest to experiment with solvents with lower (pentanol, hexanol) and higher d.c. (ethanol). However, it was impossible to differentiate between the effects of the d.c. and that of the viscosity since both varied independently in the various solvents. Fig. 48 shows that at indentical voltage and particle concentration the order of impregnation efficiency is:

isopropanol > pentanol > hexanol

(negligible impregnation was found in the SEM for ethanol and therefore no quantitative tests were performed).
It can be deduced therefore that lowering of d.c. and increase in viscosity retards particle impregnation. It should also be pointed out that the presence of ceramic particles raises the viscosity appreciably, the value increases with increase in particle concentration (see Table 4). The effect of deposition voltage on impregnation is seen in Fig. 46. A maximum at around 300V is seen for propanol at two concentrations. This can be explained by the ambivalent effect of the voltage. On one hand its increase will enhance penetration due to increase of the electric field but at the same time the build-up of the external coating which will be enhanced too will block further impregnation. Indeed at 450V a very fast build-up of external coating was observed.

The effect of concentration is seen in Fig. 47 for isopropanol at 30V. The impregnation increases with concentration with a diminishing rate.

A most interesting result was obtained during the quantitative SiO_2 determination. It was found that in those specimens where the SiO_2 concentration was at higher levels (such as 0.6%), a SiO_2 skeleton of the same shape and dimensions as the original specimen ramained after the gasification of the graphite (Fig. 49). Moreover, the cross-section of the skeleton contained SiO_2 (Fig. 50) indicating impregnation of the whole cross-section of

the graphite specimen. Thus the induction of the colloidal SiO_2 into the porous matrix under the influence of the electric field was proven.

The electroosmotic effect which enhances the filling of pores as a result of the presence of an electric field was shown in the experiments described in 4.1.3, Table 2 and Fig. 45.

The presence of an electric field has a strong influence on the penetration of water into the pores of graphite. Only 12% of the pores were filled in absence of a field, while about 80% were filled after over 5 min. but less than 15 min. of exposure, when a field of 30V/cm was applied. In the case of isopropanol 80% of filling was attained both with and without the electric field. However, the rate of filling was higher with the electric field.

Deposits of CeO_2, ZrO_2 and Al_2O_3 were obtained by cathodic reduction reactions that form OH^- followed by the interaction of the OH^- with the appropriate cation:

- electroreduction of H_2O and NO_3^-:
  $2H_2O+2e \longrightarrow H_2+2OH^-$
  $NO_3^-+H_2O+2e \longrightarrow NO_2^-+2OH^-$

- interaction between the OH^- and the cation:
  $4OH^-+Ce^{4+} \longrightarrow Ce(OH)_4$
  $3OH^-+Al^{3+} \longrightarrow Al(OH)_3$
  $4OH^-+Zr^{4} \longrightarrow Zr(OH)_4$

- Dehydration of the hydroxide to form CeO_2, Al_2O_3 and ZrO_2.

A crystallographic analysis was made for the cerium containing deposit only so far confirming the CeO_2 composition.
A similar preliminary analysis of the Zr containing deposit indicates the as-deposited material to be amorphous and to transform into the crystalline form by calcination. Thick deposits of CeO_2 and ZrO_2 could be formed by increasing c.ds. and deposition time. However, in the case of Al_2O_3 only very

thin films were obtained. This might be due to differences in the electric conductivity of the three compounds.

CHAPTER 6 - CONCLUDING REMARKS

The final objective of this research project is the development of a method for coating and impregnation of carbon-carbon composites with ceramic materials.

During this stage of the project the fundamental concepts underlying the approach, based on the phenomena of electrophoresis and electrodeposition, were tested.
Most experiments were performed, at this stage, on a model material for C-C: porous graphite.

The results obtained can be summarized as follows:

- Electrophoretic deposition of the ceramic materials, studied so far (colloidal and fused SiO_2, SiC and SiN), on graphite and C-C takes place following charging of the particles and their displacement under the influence of the electric field. The SiO_2 and SiC particles acquire a negative charge therefore are deposited on the anode, while the SiN is deposited on the cathode.

- In addition to the formation of surface deposits the induction of the ceramic particles into a porous substrate was demonstrated qualitatively for all ceramics and was studied quantitatively for colloidal SiO_2. The extent of penetration was studied on cross-sections of coated porous graphite in the SEM and by quantitative determination of the SiO_2 content in specimens obtained at various deposition conditions.

- It is shown that an optimal value exists for the deposition voltage resulting from its ambivalent effect on particle penetration. This value was found to be around 300V (180 V/cm).

- The effect of the solvents studied on impregnation efficiency in decreasing order is:

  propanol > pentanol > hexanol > ethanol

- Increase of particle concentration enhances impregnation up to about 30 g/l for colloidal SiO_2.

- Although the weight percentages of impregnated SiO_2 are low, it is shown that the whole cross-section of the porous graphite was impregnated. This is demonstrated by the SiO_2 skeleton left behind after gasification of the graphite.

- Further optimization of deposition parameters will lead to increase of extent of impregnation.

- The electroosmotic flow of isopropanol and of water into the pores was demonstrated.

- Ceramic coatings of CeO_2, ZrO_2 and Al_2O_3 were deposited on graphite and C-C by electroreduction of aqueous solutions containing inorganic salts of the appropriate metals. Clusters of CeO_2 were obtained in the skeleton of C-C by this method.

- It is shown that an optimal value exists for the deposition voltage resulting from its ambivalent effect on particle penetration. This value was found to be around 300V (180 V/cm).

- The effect of the solvents studied on impregnation efficiency in decreasing order is:

  propanol > pentanol > hexanol > ethanol

- Increase of particle concentration enhances impregnation up to about 30 g/l for colloidal SiO_2.

- Although the weight percentages of impregnated SiO_2 are low, it is shown that the whole cross-section of the porous graphite was impregnated. This is demonstrated by the SiO_2 skeleton left behind after gasification of the graphite.

- Further optimization of deposition parameters will lead to increase of extent of impregnation.

- The electroosmotic flow of isopropanol and of water into the pores was demonstrated.

- Ceramic coatings of CeO_2, ZrO_2 and Al_2O_3 were deposited on graphite and C-C by electroreduction of aqueous solutions containing inorganic salts of the appropriate metals. Clusters of CeO_2 were obtained in the skeleton of C-C by this method.

17. S. Srinivasan, H.D. Hurwitz, J.O.M. Bockris, J. Chem. Phys. 46, 3108(1967).

18. G.M. Brown, F.A. Posey, J. Electrochem. Soc. 128,(2),306 (1981).

19. B.G. Ateya, L.G. Austin, ibid, 124(11), 1590(1977).

20. J.A. Trainham, J. Newman, ibid, 124(10),1528 (1977).